© 2019. Published by The Company of Biologists Ltd | Development (2019) 146, dev172502. doi:10.1242/dev.172502

STEM CELLS AND REGENERATION

RESEARCH ARTICLE

The Shh receptor Boc is important for myelin formation and repair

Mary Zakaria[1], Julien Ferent[2], Ines Hristovska[3], Yousra Laouarem[1], Amina Zahaf[1], Abdelmoumen Kassoussi[1], Marie-Eve Mayeur[3], Olivier Pascual[3], Frederic Charron[2] and Elisabeth Traiffort[1,*]

ABSTRACT

Myelination leads to the formation of myelin sheaths surrounding neuronal axons and is crucial for function, plasticity and repair of the central nervous system (CNS). It relies on the interaction of the axons and the oligodendrocytes: the glial cells producing CNS myelin. Here, we have investigated the role of a crucial component of the Sonic hedgehog (Shh) signalling pathway, the co-receptor Boc, in developmental and repairing myelination. During development, *Boc* mutant mice display a transient decrease in oligodendroglial cell density together with delayed myelination. Despite recovery of oligodendroglial cells at later stages, adult mutants still exhibit a lower production of myelin basic protein correlated with a significant decrease in the calibre of callosal axons and a reduced amount of the neurofilament NF-M. During myelin repair, the altered OPC differentiation observed in the mutant is reminiscent of the phenotype observed after blockade of Shh signalling. In addition, *Boc* mutant microglia/macrophages unexpectedly exhibit the apparent inability to transition from a highly to a faintly ramified morphology *in vivo*. Altogether, these results identify Boc as an important component of myelin formation and repair.

KEY WORDS: Myelin, Oligodendrocyte, Axon, Hedgehog signalling

INTRODUCTION

Myelination in vertebrates is fundamental for the rapid conduction of action potentials along axons, and stands as a crucial regulator of function, plasticity and repair in the central nervous system (CNS) (Fields, 2008; Tomassy et al., 2016). This complex process relies on reciprocal interactions between neurons and oligodendrocytes: the CNS myelin-forming cells. Oligodendrocytes are the progeny of oligodendrocyte precursor cells (OPCs) and arise in multiple waves (Kessaris et al., 2006). In the dorsal forebrain, a major wave of OPC production arises from the germinative zone located just beneath the developing corpus callosum at the perinatal period. This wave coincides with the bulk of myelination occurring early after birth (Kessaris et al., 2006; Tong et al., 2015; Azim et al., 2016; Naruse et al., 2016). OPCs are maintained in the adult CNS, continue to divide, and generate new myelinating oligodendrocytes that participate in the myelin-remodelling (Young et al., 2013) and the learning processes (Gibson et al., 2014; McKenzie et al., 2014). Importantly, these progenitors also constitute a major reserve of cells scattered throughout the whole CNS that are able to be recruited towards a demyelinated area, which leads to myelin regeneration (Lopez Juarez et al., 2016; Franklin and Ffrench-Constant, 2017).

The type l transmembrane receptor Boc (brother of Cdo) is related to cell-adhesion molecules of the immunoglobulin superfamily and was initially implicated in the positive regulation of myogenic differentiation (Kang et al., 2002). Besides this role, Boc is a target and signalling component of the sonic hedgehog (Shh) pathway (Tenzen et al., 2006; Allen et al., 2011; Sanchez-Arrones et al., 2012; Yam and Charron, 2013). By binding Shh with high affinity, Boc transduces Shh signal in the guidance of commissural axons in the embryonic spinal cord (Okada et al., 2006; Tenzen et al., 2006) and in the segregation of ipsilateral retinal ganglion cell axons at the optic chiasm (Fabre et al., 2010). Later during postnatal development, Boc forms a Shh receptor complex with the main receptor patched 1 and is required for Shh-mediated cell proliferation of cerebellar granule neuron progenitors (Izzi et al., 2011). Finally, the strong expression of Boc in neurons of the cerebral cortex revealed its requirement for circuit-specific synapse formation (Harwell et al., 2012).

Recently, the Shh signalling pathway has been implicated in oligodendrocyte and myelin production during development and repair. A Shh-dependent domain in the germinal zone of the dorsal forebrain was found to produce large numbers of oligodendroglial lineage cells in the postnatal brain (Tong et al., 2015). Moreover, we and others have shown that modulation of Shh signalling can promote myelin repair (Ferent et al., 2013; Samanta et al., 2015; Sanchez et al., 2018). However, the role of Boc in oligodendrogenesis and myelination remains unexplored.

Here, we have examined the endogenous expression and function of Boc during OPC and myelin production, and in the context of CNS demyelination. During development, we show that, besides its previously described expression in callosal projection neurons, Boc can be detected in progenitors arising from the dorsal forebrain that are fated to the glial cell lineage. The *Boc*-null mutant revealed a transient oligodendroglial phenotype that delayed myelination and was associated with a decrease in the calibre of callosal axons. In the context of CNS demyelination, we demonstrate a high upregulation of *Boc* in the lesion. Together with the impaired myelin regeneration reminiscent of the phenotype observed when Shh signalling is inhibited, *Boc* mutant mice reveal morphological differences of microglia and/or macrophages *in vivo*, suggesting an inability to switch from a highly to a faintly ramified morphology. Altogether, this work identifies the Boc receptor as a new regulator of developmental myelination and remyelination.

RESULTS

Boc is expressed in neurons and neural progenitors that are fated to the glial cell lineage

The first two postnatal weeks correspond to an intense period of production and differentiation of OPCs derived from the germinative zone of the dorsal forebrain and leading to active myelination in the

[1]INSERM-University Paris-Sud/Paris-Saclay; Diseases and Hormones of the Nervous System, U1195, 80 rue du Général Leclerc, F-94276, Le Kremlin-Bicêtre, France. [2]IRCM, Molecular Biology of Neural Development, 110 Pine Avenue West, Montreal, Quebec H2W 1R7, Canada; Department of Medicine, University of Montreal, Montreal, Quebec, Canada; McGill University, Montreal, Quebec, Canada. [3]Institut NeuroMyoGène CNRS UMR 5310-INSERM U1217-Université Claude Bernard Lyon 1, Faculté de Médecine et de Pharmacie 69008 Lyon, France.

*Author for correspondence (elisabeth.traiffort@inserm.fr)

J.F., 0000-0002-4659-230X; E.T., 0000-0002-9645-6269

Received 6 October 2018; Accepted 28 March 2019

Development (2019) 146, dev172502. doi:10.1242/dev.172502

rodent brain (Kessaris et al., 2006). On day 8 after birth (P8), the highest Boc expression was detected in the cerebral cortex, and in the external granular and Purkinje cell layers of the cerebellum, as previously described (Izzi et al., 2011; Harwell et al., 2012). In addition, Boc could be observed in the germinative zone located just beneath the developing subcortical white matter (Fig. 1A). This area comprises undifferentiated progenitors, which give rise to oligodendroglial lineage cells that notably migrate to and populate the developing corpus callosum and the cerebral cortex during the first postnatal weeks (Menn et al., 2006; Seri et al., 2006; Kim et al., 2011; Azim et al., 2016; Naruse et al., 2016). At P8, in the germinative zone, 79±3% of Boc$^+$ cells co-expressed the proliferation marker Ki67 (Fig. 1B,D), while 32±2% were labelled for the Olig2 marker (Fig. 1C,D), which at this developmental stage is expressed in both oligodendrocyte and astrocyte progenitors (Naruse et al., 2017). Remarkably, most Olig2$^+$ cells detected at a distance from the germinative area were devoid of Boc expression (white arrowheads in Fig. 1C). At P15, Boc-expressing cells were mainly observed in layers II to V of the cerebral cortex (Fig. 1E). The majority of these cells (97±1%) co-expressed the marker of mature neurons NeuN and corresponded to 58.5±4.9% of the neuronal population (Fig. 1F and data not shown). The remaining 3±1% co-expressed Olig2 and constituted only 2±1% of all the Olig2$^+$ oligodendroglial cells in the cortex (Fig. 1G,H). In the corpus callosum, a faint Boc immunofluorescence was detected in the cytoplasm of a few scattered cells co-expressing Olig2 and the adenomatous polyposis coli (APC/CC1) marker. Boc$^+$ cells represented only 15±2% of the oligodendroglial population in the corpus callosum at P15 (Fig. 1H). Given the decrease of Boc immunostaining from P8 to P15, we investigated Boc expression at earlier time points (Fig. 1I). *In situ* hybridization led to the detection of a high level of *Boc* transcription at P0 and P5 in the dorsal germinative zone. A much weaker signal

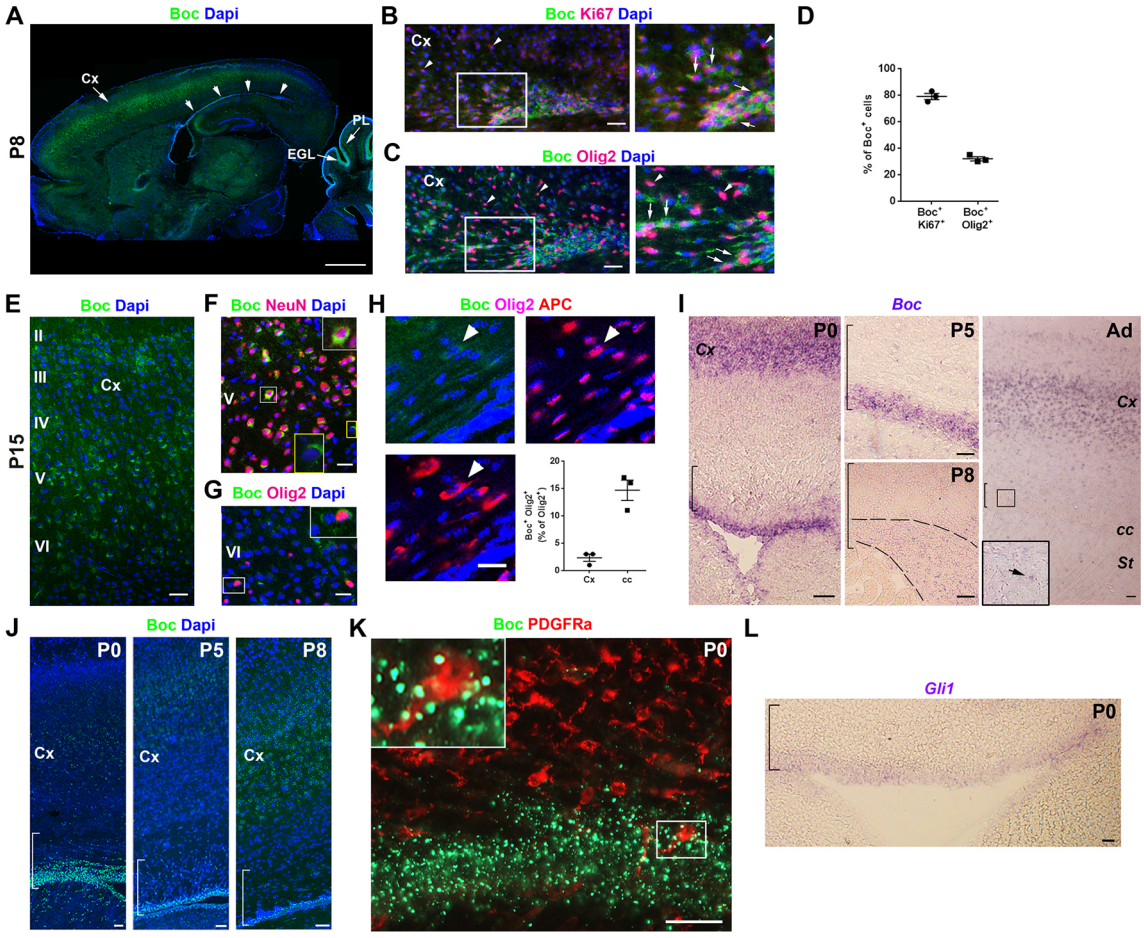

Fig. 1. Boc is expressed in neurons and neural progenitors of the dorsal forebrain germinative zone. (A) Tiled image visualizing Boc immunoreactivity in the P8 mouse brain. The four white arrows indicate the germinative zone of the dorsal forebrain. (B,C) Double immunohistofluorescence at the level of the germinative zone showing Boc$^+$ cells co-expressing (white arrows) or not (white arrowheads) the proliferation and oligodendroglial markers Ki67 and Olig2, respectively. The right panels are magnifications of the boxed areas. (D) Quantification of Boc$^+$ Ki67$^+$ and Boc$^+$ Olig2$^+$cells. (E-G) Visualization of Boc expression in the cerebral cortex from a P15 mouse (E, cortical layers are indicated on the left) and its co-expression with markers of mature neurons (NeuN, F) and of oligodendroglial cells (Olig2, G). Insets show boxed areas at higher magnification. (H) Triple immunostaining using Boc, Olig2 and APC antibodies visualizes a Boc$^+$ cell co-expressing Olig2 and APC in the corpus callosum at P15 (white arrowhead). The graph shows the quantification of the percentage of Olig2$^+$ cells co-expressing Boc in the cerebral cortex or corpus callosum. (I) *Boc in situ* hybridization of brain slices from P0, P5, P8 and adult mice at the level of the dorsal germinative zone. The dotted lines delineate the germinal zone at P8. The boxed area in the adult shows a scattered Boc$^+$ cell in the corpus callosum. (J) Boc immunostaining of brain slices from P0, P5 and P8 *Boc* knockout mice. (K) Boc$^+$ and PDGFRa$^+$ immunostaining in the dorsal germinative zone and developing corpus callosum in the P0 *Boc* mutant. The boxed area indicates an OPC still present in the germinative zone and likely expressing Boc (yellow puncta). (L) *Gli1 in situ* hybridization in the dorsal germinative zone at P0. The brackets in I,J,L indicate the position of the germinative zone and developing corpus callosum. Scale bars: 500 µm in A; 50 µm in B,C,E,H-L; 25 µm in F,G. Data are mean±s.e.m. cc, corpus callosum; Cx, cerebral cortex; EGL, external granular cell layer; PL, Purkinje layer; St, striatum.

Development (2019) 146, dev172502. doi:10.1242/dev.172502

was observed at P8 and became restricted to a few scattered cells in the corpus callosum of the adult animal (boxed area in Fig. 1I). In contrast, Boc$^+$ cells were clearly detected at all time points in the cerebral cortex (Fig. 1I and data not shown). To improve the visualization of low Boc protein levels, we took advantage of the insertion of a gene-trap β-galactosidase cassette inside the Boc gene of the *Boc* mutant mouse strain (Okada et al., 2006). A fragment of the N-terminal extracellular domain of Boc is still expressed in these mutants. We have shown previously that the Boc antibody reacts with this inactive fragment, which is retained intracellularly but inactive, and that the signal from this antibody disappears in *Boc*-null mutant mice (Allen et al., 2011). Therefore, we immunostained brain slices derived from P0, P5 and P8 mutant mice. In agreement with *in situ* hybridization experiments, we detected a high Boc signal in the dorsal germinative zone from P0 pups progressively decreasing until P8 (Fig. 1J). Moreover, double immunostaining of mutant P0 brain slices by using antibodies against Boc and PDGFRa, a marker of OPCs, showed that most OPCs were devoid of Boc expression, although we could not completely exclude the possibility that a subset may maintain Boc expression (boxed area in Fig. 1K). Remarkably, transcripts of Gli1, the transcriptional effector of Shh signalling, were also detected at a low level in the P0 dorsal germinative zone (Fig. 1L). These data thus indicate that, besides its neuronal expression during the early postnatal period, Boc is present in proliferating progenitors of the dorsal germinative zone.

Boc regulates the perinatal production of undifferentiated neural progenitors and OPCs

The expression of Boc in progenitors of the dorsal germinal zone during the period of oligodendrocyte production raised the possibility that Boc could be involved in the dorsal wave of oligodendrogenesis. To test this hypothesis, we analysed *Boc* mutant mice and immunolabelled P0 forebrain sections derived from wild-type and *Boc* mutant pups for Olig2 and the neural stem cell marker Sox2 (Ellis et al., 2004; Dai et al., 2015). In the germinative zone of the dorsal forebrain, the neural progenitors co-express both markers, but progressively reduce Sox2 expression while they migrate towards the developing subcortical white matter and commit into astro- or oligodendroglial progenitors. As expected, immediately after birth, we observed a high number of Sox2$^+$ and Olig2$^+$ cells in the developing subcortical white matter from the wild-type animals (Fig. 2A). Olig2$^+$ cells co-expressed either a high or a low level of Sox2, reflecting the ongoing reduction in Sox2 expression (Fig. 2A, top, inset). In the P0 *Boc* mutant animals, we observed a significant decrease in the density of Sox2$^+$ (132±13 versus 210±12 cells/0.1 mm^2, P=0.002) and Olig2$^+$ (92±8 versus 164±7 cells/0.1 mm^2, P=0.0005) cells compared with the wild-type animals (Fig. 2A,B). However, the proportion of Sox2$^+$ neural progenitors upregulating Olig2 was not changed, suggesting that the absence of Boc reduced the production of Sox2$^+$ neural progenitors but not their commitment into Olig2$^+$ progenitors.

Although Boc was mostly expressed in neural progenitors and not in OPCs, we next tested whether the absence of Boc in the former may nevertheless alter the proliferation of OPCs. Therefore, we immunostained P0-P1 slices with the OPC and proliferation markers PDGFRa and Ki67, respectively. The density of PDGFRa$^+$ OPCs was significantly decreased in *Boc* mutant compared with the wild-type pups (140±15 versus 196±18 cells/0.1 mm^2, P=0.04). The proportion of proliferating PDGFRa$^+$ Ki67$^+$ cells was also decreased (31±5 versus 42±2%, P=0.03) not only at P0 (Fig. 2C,D) but also at P5 (Fig. 2E,F). In contrast, this percentage collapsed at P8 in the wild-type animals (20±2 versus 49±3%, P=0.0001), whereas it remained stable in the mutant (33±1 versus 29±4%) (Fig. 2E,F), suggesting a prolonged OPC proliferation in the mutant beyond that observed in wild-type animals. To determine whether Boc may be involved in the previously reported Shh-mediated proliferation of OPCs, we used a mixed glial cell culture containing astrocytes, oligodendroglial cells and microglia derived from the dorsal forebrain of P0-P1 wild-type and *Boc* mutant pups. In agreement with the reduced number of oligodendroglial cells generated in the dorsal germinal zone of the mutants, the percentage of Olig2$^+$ cells was significantly reduced (18.5±1.1 versus 28.8±3.2%, P=0.023; Fig. 2G,H). Two hours after a short pulse of the proliferation marker BrdU, we observed a lower percentage of Olig2$^+$ cells able to incorporate BrdU in the mutant than in the wild type (11.5±0.8 versus 19.3±0.7%; P=0.0002). Moreover, supplementation of the culture medium with recombinant Shh protein (4 nM), which is able to bind its receptor complex (Izzi et al., 2011), significantly increased the percentage of wild-type Olig2$^+$ BrdU$^+$ cells (29.1±2.4 versus 19.3±0.7%, P=0.002). In contrast, Shh stimulation only slightly and non-significantly increased the proliferation of OPCs derived from *Boc* mutants (13.0±0.5 versus 11.5±0.8%) (Fig. 2G,H). *Gli1* transcription was increased by about fourfold when Shh was added to the wild-type cells (4.4±0.8 versus 1.2±0.5, P=0.02), although it was not significantly upregulated when Shh was added to the mutant cell culture (2.1±0.5 versus 1.3±0.4; Fig. 2I), suggesting that Boc is required in neural progenitors from the dorsal germinative zone for their progeny to respond to Shh. In a consistent manner, Gli1 transcription level determined by quantitative RT-PCR in the forebrain from wild-type and Boc mutant mice indicated significant *Gli1* downregulation in P8 and P15 animals (Fig. 2J). Then, to evaluate whether mutant OPCs could be refractory to any stimulation, the mixed glial cell cultures were treated with SAG (3×10^{-7}M), an agonist of the key transducer of Shh signalling smoothened (Smo). SAG induced an increase in the percentage of Olig2$^+$ cells incorporating BrdU in both the wild-type (28±2 versus 18±1, P=0.003) and the mutant (18±2 versus 11±1, P=0.02; Fig. 2K, L) cultures, in disagreement with the idea of a full refractory state of Boc mutant progenitors. In addition, purified OPCs derived from wild-type and mutant pups responded to Shh in a similar manner to the mixed glial cell cultures (Fig. 2M,N), further supporting the hypothesis that Boc inactivation affects OPC proliferation independently of the other glial cells present in the culture.

The absence of Boc decreases MBP production in the dorsal forebrain

The decrease in OPC production at the perinatal period suggested that the absence of Boc may influence developmental myelination of axons that takes place during the first three postnatal weeks in rodents. Therefore, we performed western blot analysis using the dorsal forebrain from P8, P15 and adult wild-type or mutant mice (Fig. 3A,B). MBP protein was significantly decreased in *Boc* mutant compared with wild-type mice at P8 (0.631±0.009 versus 1.018±0.022, P<0.0001), P15 (0.807±0.018 versus 1.036±0.017, P=0.0001) and in adulthood (0.845±0.007 versus 1.093±0.04, P=0.0001). In order to determine whether MBP decrease was related to a reduced density of oligodendroglial cells throughout the whole process of developmental myelination, we first analysed the transcription of *Olig2* using quantitative RT-PCR. In *Boc* mutants, as expected, *Olig2* transcription was significantly decreased at P0-P1 (0.73±0.01 versus 1.00±0.02, P=0.005) and remained lower compared with the wild type at P8 (Fig. 3C). To further support this observation, we analysed the generation of OPCs

Development (2019) 146, dev172502. doi:10.1242/dev.172502

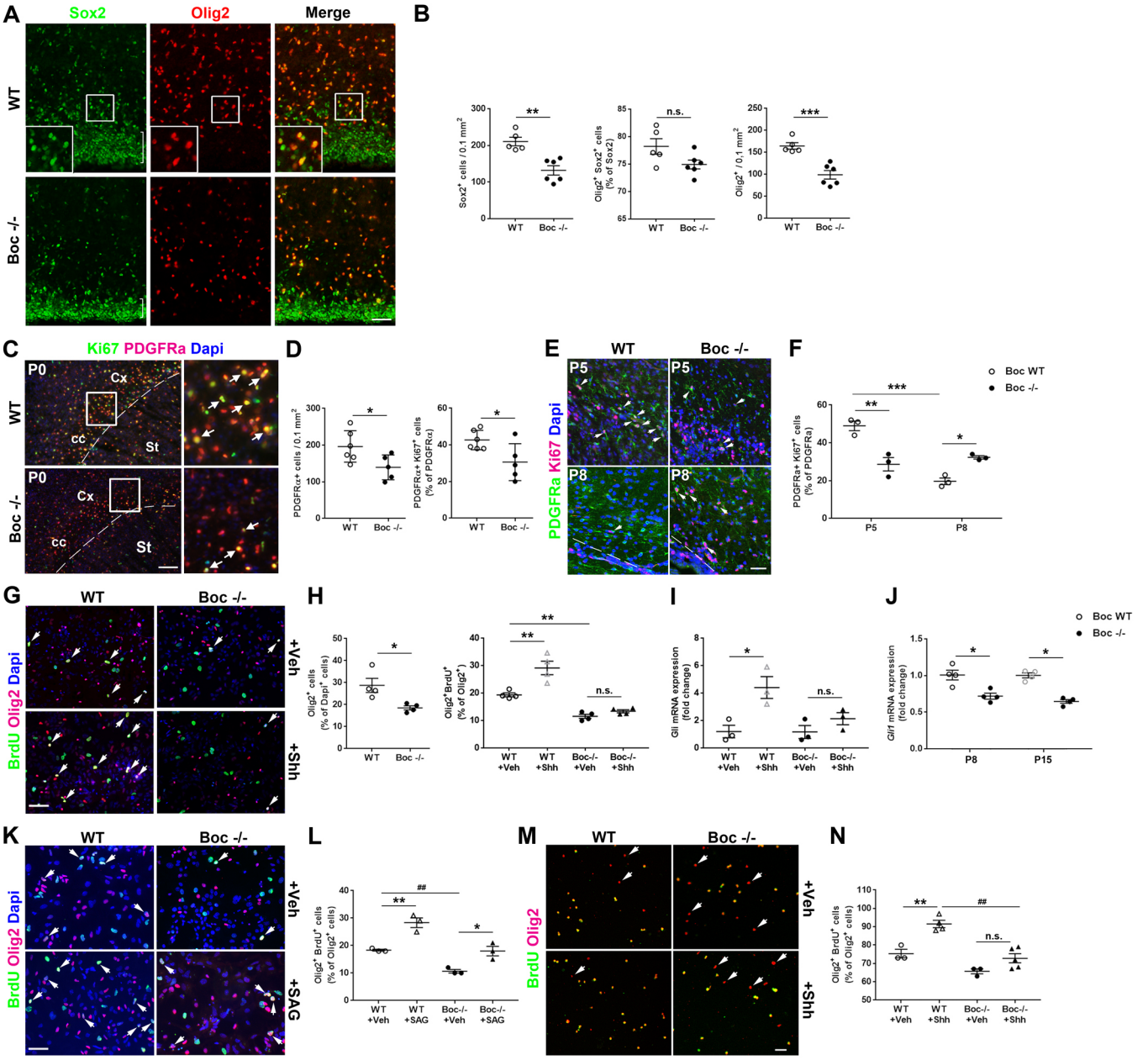

Fig. 2. Boc regulates the perinatal production of neural progenitors and OPCs. (A) Immunostaining of slices derived from P0-P1 wild-type or *Boc*$^{-/-}$ pups at the level of the germinative zone (white bracket) of the dorsal forebrain identified by Sox2 expression. Cells arising from this area and co-expressing the Olig2 marker are pre-OPCs and/or OPCs. (B) Quantification of Sox2^{+} and Olig2^{+} cells, and of the percentage of Sox2^{+} Olig2^{+} cells in the Sox2^{+} population. (C-F) Immunostaining and quantification of slices from P0-P1 (C,D), P5 and P8 (E,F) pups using Ki67 and PDGFRa as cell proliferation and OPC markers, respectively. (G,H) Primary mixed glial cell cultures derived from the forebrain of P0-P1 wild-type and *Boc*$^{-/-}$ mice assessed for cell proliferation after incorporation of the proliferation marker BrdU in the presence (+Shh) or absence (+Veh) of recombinant Shh protein. (I,J) Determination of *Gli1* transcription in the indicated culture conditions (I) and in the forebrain of P8 and P15 wild-type and *Boc*$^{-/-}$ mice (J) using quantitative RT-PCR. (K,L) Primary mixed glial cell cultures assessed for cell proliferation in the presence (+SAG) or absence (+Veh) of the Smo agonist SAG. (M,N) Purified OPCs prepared from P0-P1 wild-type and *Boc*$^{-/-}$ mice, and assessed for cell proliferation in the presence (+Shh) or absence (+Veh) of recombinant Shh protein. The white arrows show Olig2^{+} BrdU^{+} cells in G,K, PDGFRa^{+} Ki67^{+} in C,E and Olig2^{+} BrdU^{-} cells in M. Scale bars: 50 µm in E,K,M; 100 µm in A,G; 200 µm in C. Each point in the graphs corresponds to one animal or one culture. Statistical analysis used unpaired two-tailed *t*-test (B,D,H, left), two-way ANOVA and Tukey's multiple comparisons (F,H, right; I,J,L,N). **P*<0.05; ** and $^{\#\#}$*P*<0.01, ****P*<0.001; n.s. not significant. Data are mean±s.e.m.

and oligodendrocytes by immunostaining P8, P15 and adult brain slices with markers of OPCs (PDGFRa) and mature oligodendrocytes (APC). At P8, the density of PDGFRa^{+} OPCs was slightly but significantly lower in the mutant compared with the wild-type corpus callosum (Fig. 3D,E). Similarly, we observed a lower density of Olig2^{+} and APC^{+} cells. However, the percentage of APC^{+} cells in the Olig2 population (19±2 versus 22±2%) was unchanged, indicating that the absence of Boc did not alter the capacity of OPCs to differentiate into mature oligodendrocytes (Fig. 3F,G). At P15, in agreement with the absence of regulation of *Olig2* transcription observed at this age, the populations of Olig2^{+} and APC^{+} cells remained comparable in both genotypes (Fig. 3H,I). Similarly, no significant modification in the ability of OPCs to differentiate into APC^{+} oligodendrocytes was observed in

Development (2019) 146, dev172502. doi:10.1242/dev.172502

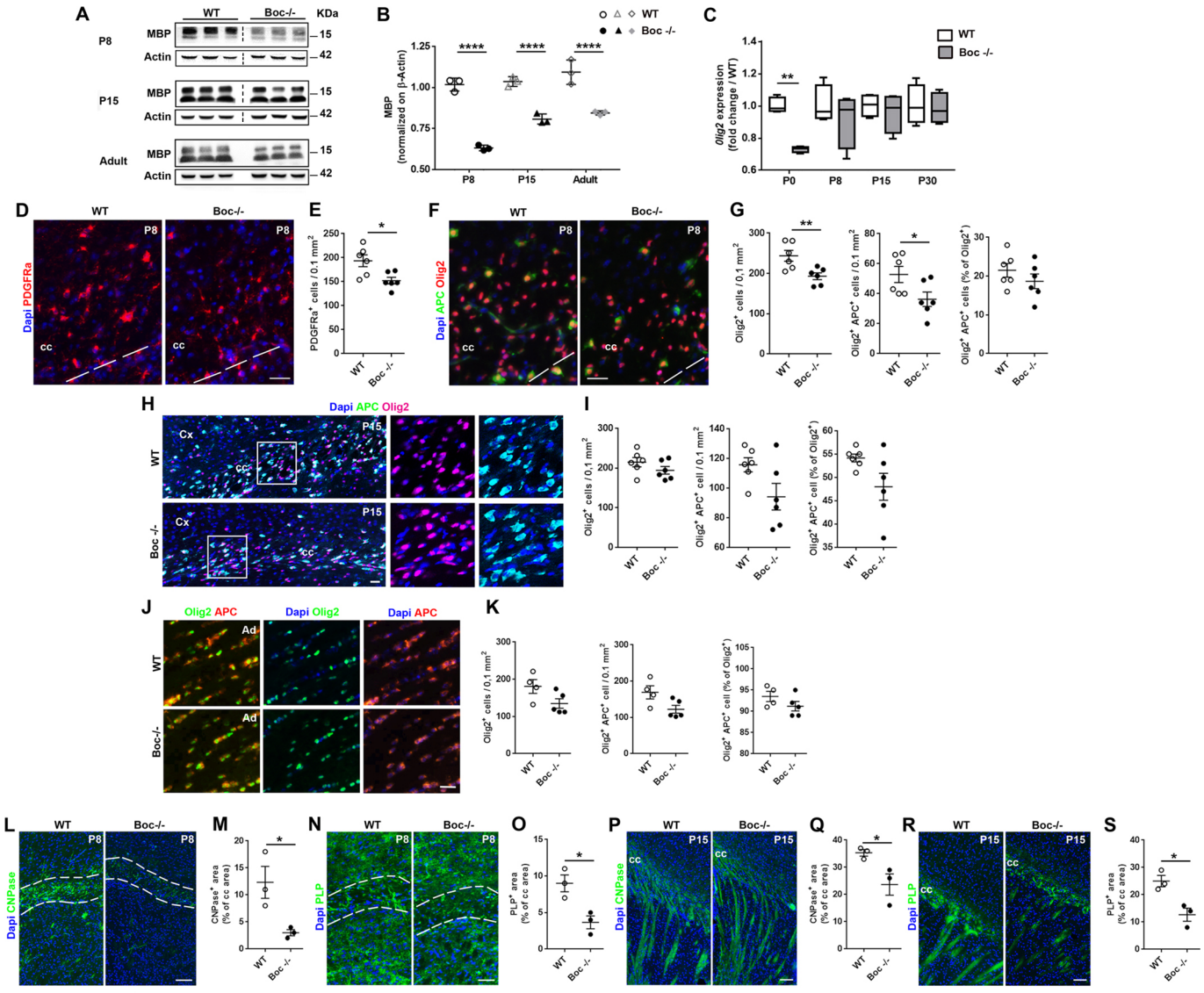

Fig. 3. Boc KO mice display a decreased production of myelin in the developing dorsal forebrain. (A) Western blot analysis of dorsal forebrain homogenates derived from P8, P15 and adult wild-type and *Boc*$^{-/-}$ mice. (B) Densitometric analysis of MBP immunoreactive signals normalized to β-actin expression. (C) *Olig2* transcript level determined by quantitative RT-PCR in the developing dorsal forebrain from P0, P8, P15 and P30 wild-type and *Boc*$^{-/-}$ mutant mice (*n*=3). Boxes and whiskers indicate minimal to maximal values and corresponding s.e.m., respectively. (D-G) PDGFRa and Olig2/APC immunostaining and corresponding quantifications carried out in slices from P8 wild-type or *Boc*$^{-/-}$ mice. The dashed line indicates the position of the germinative zone. (H-K) Visualization and quantification of Olig2^{+} cells and APC^{+} differentiated oligodendrocytes in the corpus callosum of P15 (H,I) and adult (J,K) wild-type and *Boc*$^{-/-}$ mice. (L-S) Visualization and quantification of CNPase^{+} and PLP^{+} immunostaining in the developing corpus callosum at P8 (L-O) and P15 (P-S) in wild-type and *Boc*$^{-/-}$ animals. The dashed lines in (L,N) delineate the developing corpus callosum. cc, corpus callosum; Cx, cerebral cortex. Scale bars: 50 µm in D,F,H,J,N; 100 µm in L,P,R. Statistical analysis used unpaired two-tailed *t*-test (E,G,I,K,M,O,Q,S), two-way ANOVA and Sidak's multiple comparisons (B,C). **P*<0.05; ***P*<0.01, *****P*<0.0001. Data are mean±s.e.m.

the mutant (48±3 versus 54±1%) (Fig. 3I). A similar result was obtained in adulthood, where 92±1 and 94±1% of Olig2^{+} cells co-expressed the APC marker in the mutant and wild-type corpus callosum, respectively (Fig. 3J,K). However, consistent with the decrease in MBP previously observed, visualization of other myelin proteins, including the 2′,3′-cyclic-nucleotide 3′-phosphodiesterase (CNPase) and the proteolipid protein (PLP) indicated a significantly lower level of these proteins in P8 and P15 *Boc* mutants (Fig. 3L-S) compared with wild type. Collectively, these results indicate that the decreased production of OPCs observed in *Boc* mutants at birth can still be detected at P8 but recovers from P15 onwards, in contrast to the level of myelin proteins, which remains persistently reduced.

Impaired upregulation of gelsolin and delayed myelination in *Boc* mutant mice

To further characterize the decrease in MBP protein observed at P8 and because the heterozygous *Mbp*$^{+/-}$ mice have been shown to display only a subtle hypomyelination phenotype (Poggi et al., 2016), we determined whether the decrease in MBP observed in *Boc* mutant mice was associated with abnormal myelination of axons. At this age, myelination had already started in the lateral corpus callosum of control mice, but was significantly reduced in *Boc* mutant mice (Fig. 4A), as indicated by the determination of the area occupied by MBP^{+} myelin sheaths in this region (25±1 versus 42±2%; *P*=0.0002; Fig. 4B). Consistently, the proportion of APC^{+} oligodendrocytes co-expressing MBP was significantly lower in

Development (2019) 146, dev172502. doi:10.1242/dev.172502

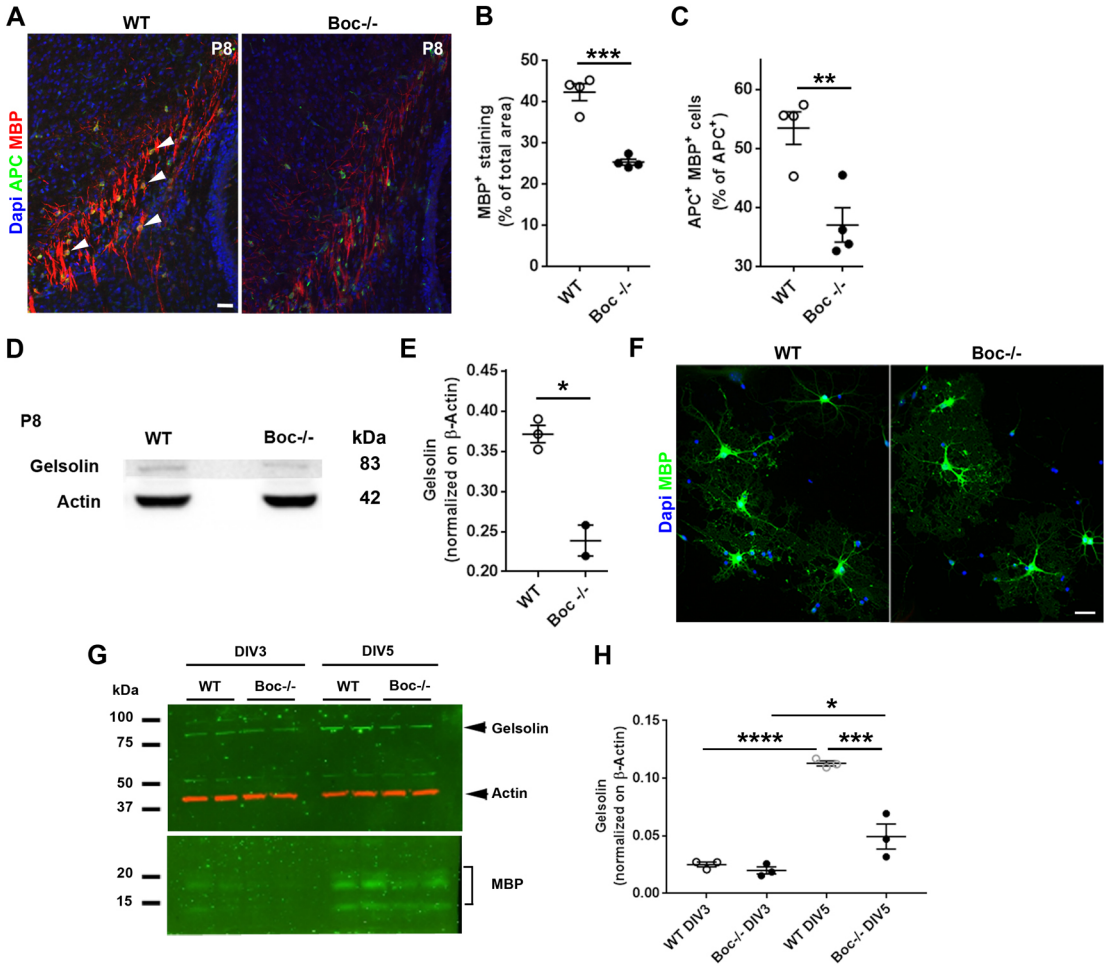

Fig. 4. The *Boc* mutant fails to induce actin disassembly proteins and leads to a delay of myelination. (A) Initiation of myelination detected by MBP upregulation in APC$^+$ oligodendrocytes and first MBP$^+$ myelin sheaths occurring in P8 wild-type and mutant mice. White arrowheads indicate APC$^+$ MBP$^+$ cells in the wild-type developing corpus callosum. (B,C) Quantification of the area occupied by MBP and the percentage of APC$^+$ MBP$^+$ cells in each genotype. (D) Detection of gelsolin immunoreactivity by western blot analysis of dorsal forebrain homogenates derived from P8 wild-type and *Boc*$^{-/-}$ mice. (E) Densitometric analysis of gelsolin signals normalized to β-actin expression. (F) Oligodendrocyte-enriched cultures prepared from the dorsal forebrain of wild-type or *Boc* mutant pups immunostained with MBP after 3 DIV show no major morphological differences. (G) Western blot analysis evaluating gelsolin and MBP expression in these cultures at 3 and 5 DIV. (H) Densitometric analysis of the immunoreactive gelsolin signal normalized to β-actin expression. Scale bars: 50 µm. Statistical analysis used unpaired two-tailed *t*-test (B,C,E), two-way ANOVA and Tukey's multiple comparisons (H). **P*<0.05, ***P*<0.01, ****P*<0.001. Data are mean±s.e.m.

Boc mutants compared with controls (37±3 versus 53±3%; *P*=0.006; Fig. 4C). Moreover, the release of gelsolin, one of the proteins required for oligodendrocyte actin disassembly, which is a step that is necessary to promote myelin wrapping around axons (Zuchero et al., 2015), was also reduced in the mutant. Indeed, forebrain homogenates from P8 wild-type or mutant animals analysed by western blot revealed a slight but significant decrease of gelsolin in the mutant (0.238±0.019 versus 0.371±0.011; *P*=0.04; Fig. 4D,E). In addition, we evaluated the ability of enriched oligodendrocyte cultures to differentiate for 5 DIV. No major morphological differences (Fig. 4F) were observed according to the genotype, suggesting that the absence of Boc in the neural progenitors did not impair the ability of OPCs to differentiate into oligodendrocytes. However, western blot analysis of such cultures at DIV 3 and DIV 5 revealed an increase in gelsolin signal in both genotypes from DIV 3 to DIV 5, with a much lower upregulation of gelsolin in the mutant (0.04±0.01 versus 0.11±0.01; *P*=0.0001; Fig. 4G,H). Thus, in *Boc* mutants, the delayed production of OPCs at birth is correlated with a decrease in MBP production and a defective gelsolin upregulation, both of which are consistent with the delay in developmental myelination observed at P8.

The absence of *Boc* causes/is associated with a decrease in myelinated axon calibre

Despite the recovery of regular oligodendroglial density in adult *Boc* mutants, the persistent decrease in MBP production remained intriguing. Therefore, we analysed the adult corpus callosum at the ultrastructural level. A striking observation was that axons appeared smaller in *Boc* mutants compared with wild-type corpus callosum (Fig. 5A,B). The analysis of more than 1000 axons from the three animals studied for each genotype indicated that the total number of axons was not significantly different in *Boc* mutants compared with wild-type animals (135±9 versus 128±11 axons per 100 µm^2; Fig. 5C). In a similar manner, no significant difference was found in the proportion of myelinated axons (68±3 versus 62±3%; Fig. 5D). In contrast, the mean diameter evaluated for 200 wild-type and 150 *Boc* mutant myelinated axons was significantly lower in the mutants (0.574±0.033 versus 0.773±0.061; *P*=0.047; Fig. 5E). Characterized as a structure containing mainly small-calibre axons

Development (2019) 146, dev172502. doi:10.1242/dev.172502

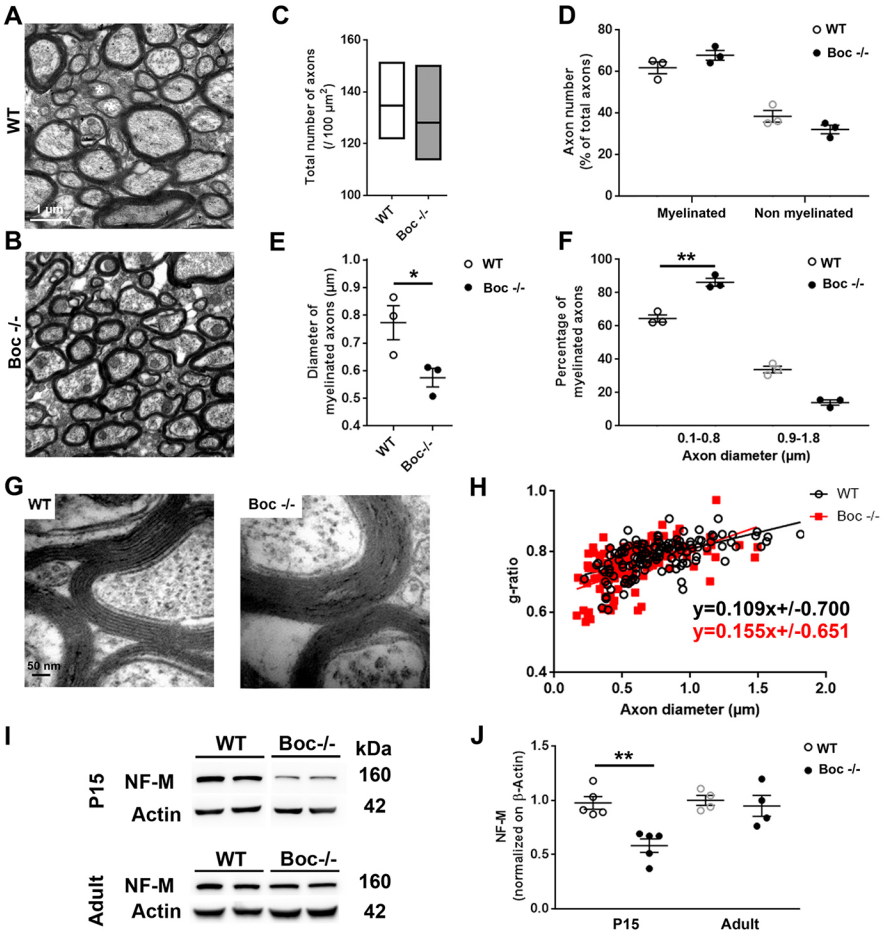

Fig. 5. The absence of Boc induces a decrease in the diameter of axons. (A,B) Visualization of coronal sections of the corpus callosum derived from wild-type (A) or *Boc*$^{-/-}$ (B) adult mice using electron microscopy. (C,D) The total number of axons (C, *n*=3 mice) and the percentage of myelinated axons (D) do not significantly differ according to the genotype. Boxes indicate minimal to maximal values in C. (E) The diameter of myelinated axons is decreased in the mutant animals. (F) The mutant displays a significantly higher proportion of myelinated axons with a diameter in the range 0.1-0.8 µm at the expense of larger calibre axons. (G,H) Visualization of myelin sheaths at high magnification and linear regression of the g-ratio (axon diameter/axon+myelin diameter). (I) Western blot analysis of the neurofilament NF-M in the dorsal forebrain from P15 and adult wild-type or *Boc* mutant animals. (J) Densitometric analysis of NF-M immunoreactive signals normalized to β-actin expression. Statistical analysis used unpaired two-tailed *t*-test (C-F,J). *P<0.05; **P<0.01. Data are mean±s.e.m.

(Hildebrand et al., 1993), the corpus callosum from the wild-type mice contained a high percentage of axons narrower than 0.8 µm. Remarkably, this percentage was even higher in the mutant (86±2 versus 65±2%; P=0.002) at the expense of axons with a diameter in the range 0.9-1.8 µm (14±2 versus 34±2; Fig. 5A,B,F). The g-ratio (the ratio of the axon diameter to axon+myelin diameter) was determined and the values were plotted against the axon diameter from n=134 and n=119 axons derived from three animals of each genotype (Fig. 5G,H). The equations were y=0.155x+0.651 and y=0.109x+0.700 for *Boc* mutants and wild type, respectively. The differences observed in the slopes and the intercepts did not reached significance (P=0.06). Because of the role of the neurofilament medium NF-M recognized in the control of axon calibre mostly in the peripheral nervous system, we looked for a change in the expression level of NF-M using western blot analysis. Consistent with the globally reduced axon calibre, *Boc* mutants showed a significantly reduced amount of NF-M at P15 (0.573±0.064 versus 0.927±0.077; P=0.008). In adulthood, no significant difference was observed (0.948±0.096 versus 1.000±0.046). Taken together, these results indicate that, in adulthood, the reduced production of MBP is not associated with hypomyelination, but could be the indirect result of the decreased axon diameter in *Boc* mutants. Moreover, the absence of Boc is associated with a reduced amount of the neurofilament NF-M.

The absence of Boc prevents spontaneous remyelination in LPC-treated animals

Given the oligodendroglial phenotype of the *Boc* mutant during development, we evaluated the possible consequences of inactivating *Boc* in the spontaneous regeneration of myelin that occurs upon demyelination. We used a model based on the injection of lysolecithin (LPC) into the corpus callosum. In this model, repair of the tissue comprises several successive and stereotyped steps, including the recruitment and proliferation of OPCs (at 5 days post-lesion, dpl), their differentiation into immature oligodendrocytes (at 10 dpl) and their maturation into myelinating cells (at 15 dpl). This process finally leads to the regression of the lesion size. We compared the main steps of the remyelination process in the corpus callosum from wild-type and *Boc* mutant animals. At 5 dpl, while Olig2$^+$ cells have already populated the demyelinated area in the wild-type mice, only rare Olig2$^+$ cells could be detected in the lesion from *Boc* mutants, indicating altered/delayed recruitment of new oligodendroglial cells. In a consistent manner, at 10 dpl, the density of differentiated APC$^+$ oligodendrocytes was largely reduced in the lesion from *Boc* mutants compared with wild type (Fig. 6A). The quantification of Olig2$^+$ and APC$^+$ cells at the different steps of the regeneration process confirmed a significantly lower density of oligodendroglial lineage cells in the mutant lesion until 15 dpl. However, at a later time point (21 dpl), the difference was largely attenuated, suggesting that Boc delays rather than impedes OPC recruitment (Fig. 6B). In contrast, the absence of Boc appeared to prevent OPC differentiation, as APC$^+$ immature oligodendrocytes were detected at a much lower level in the mutant than in the wild type at all time points. APC$^+$ cells reached a plateau between 15 and 21 dpl, representing 60-70% of the level observed in the wild type (Fig. 6C). In agreement with the delay for recruiting new Olig2$^+$ cells, the number of PDGFRa$^+$ OPCs (43±2 versus 72±5; P=0.001) and the percentage of proliferating OPCs (13±1 versus 18±2%;

Development (2019) 146, dev172502. doi:10.1242/dev.172502

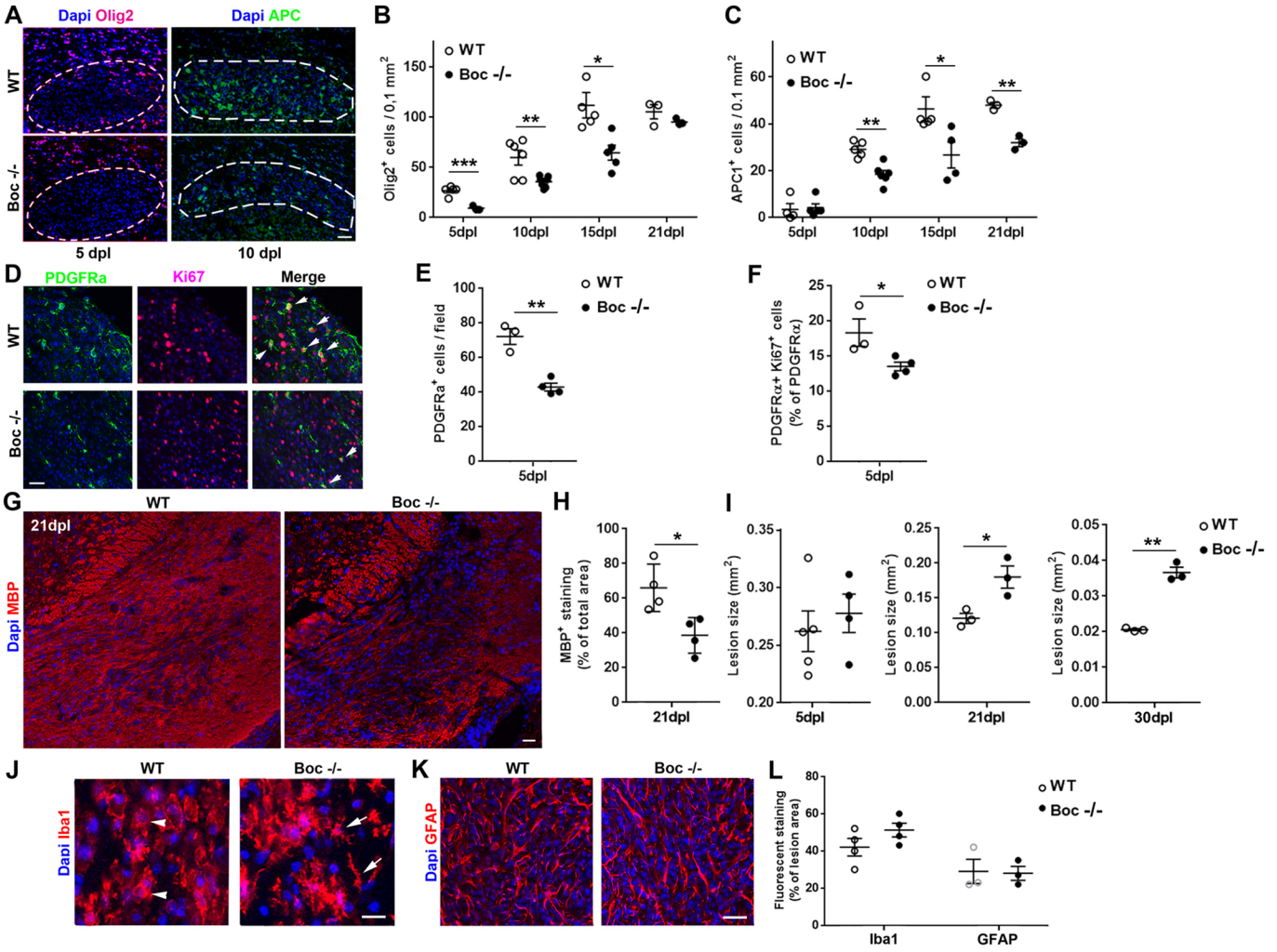

Fig. 6. The absence of functional Boc impedes complete remyelination. (A) Visualization of Olig2$^+$ and APC$^+$ cells in the lesion after the stereotaxic injection of LPC into the corpus callosum of wild-type and *Boc* mutant mice. The white dotted lines delineate the lesion. (B,C) The histograms show the densities of Olig2$^+$ (B) and APC$^+$ (C) cells quantified in the lesion of the wild-type and mutant mice at the indicated time points. (D-F) Double immunostaining using PDGFRa and Ki67 in the lesion at 5 dpl (D) and quantifications of the density of OPCs and the percentage of proliferating OPCs (E,F). Arrows in D indicate double-labelled cells. (G) Immunodetection of MBP in the lesion from the wild-type and mutant mice at 21 dpl. (H) The determination of MBP immunofluorescent area is shown in the histogram. (I) Evaluation of the lesion size at 5, 21 and 30 dpl. (J-L) Visualization of Iba1$^+$ microglia and GFAP$^+$ astrocytes at 10 dpl in the lesion from the wild-type and mutant mice. (J) Microglia and/or macrophage morphology appears more ameboid in the wild type (arrowheads) and more multipolar (arrows) in the mutant. (K) In contrast, no morphological differences are observed for astrocytes. (L) Quantification of Iba1 and GFAP fluorescent areas indicates no significant difference according to the genotype. Scale bars: 100 µm in A; 50 µm in D,G,K; 25 µm in J. Statistical analysis used multiple *t*-test (B,C) and unpaired two-tailed *t*-test (E,F,H,I,L). **P*<0.05; ***P*<0.01. Data are mean±s.e.m.

P=0.04; Fig. 6D,E,F) were decreased in the mutant at 5 dpl. Moreover, in a manner consistent with the impairment of OPC differentiation, *Boc* mutants displayed a lower ability to repair myelin, as indicated by the significantly lower MBP immunolabelling in the demyelinated area at 21 dpl (38±5 versus 66±6%, *P*=0.02; Fig. 6G,H). The lesion size was also determined by measuring the area in which a high cell nuclei density persists or the area devoid of small chains of cells compared with the unlesioned corpus callosum. Although the extent of the lesion significantly decreased in both the wild-type and mutant animals between 5 and 30 dpl, the lesion remained significantly larger in the mutant at 21 (0.180±0.016 versus 0.121±0.007 mm^2, *P*=0.03) and 30 dpl (0.035±0.003 versus 0.021±0.001 mm^2; *P*=0.001) (Fig. 6I).

Finally, we immunolabelled astrocytes and microglia and/or macrophages using Iba1 and GFAP markers in each animal group. Both cell types were detected in *Boc* mutants, as shown at 10 dpl (Fig. 6J-L), suggesting that the absence of Boc did not prevent the astro- and microgliosis in the lesion. However, microglia and/or macrophages appeared to display some discrete morphological differences, with cells apparently more ameboid in the wild type and more multipolar in *Boc* mutants (Fig. 6J). In contrast, no morphological differences could be observed for astrocytes (Fig. 6K). Moreover, the extent of the response determined by the measure of the area occupied by Iba1 and GFAP fluorescent signals did not differ according to the genotype. *In situ* hybridization using the *Boc* riboprobe showed that, as early as 2 dpl, *Boc* was upregulated not only at the site of LPC injection, but also in the ipsilateral SVZ compared with the contralateral hemisphere (Fig. 7A,B). Co-immunolabelling of the slices with the Olig2 marker indicated that some *Boc*$^+$ cells co-expressed Olig2 both in the lesion and in the SVZ (Fig. 7C), suggesting that, besides the reduced proliferation of OPCs shown above, OPC migration from

Development (2019) 146, dev172502. doi:10.1242/dev.172502

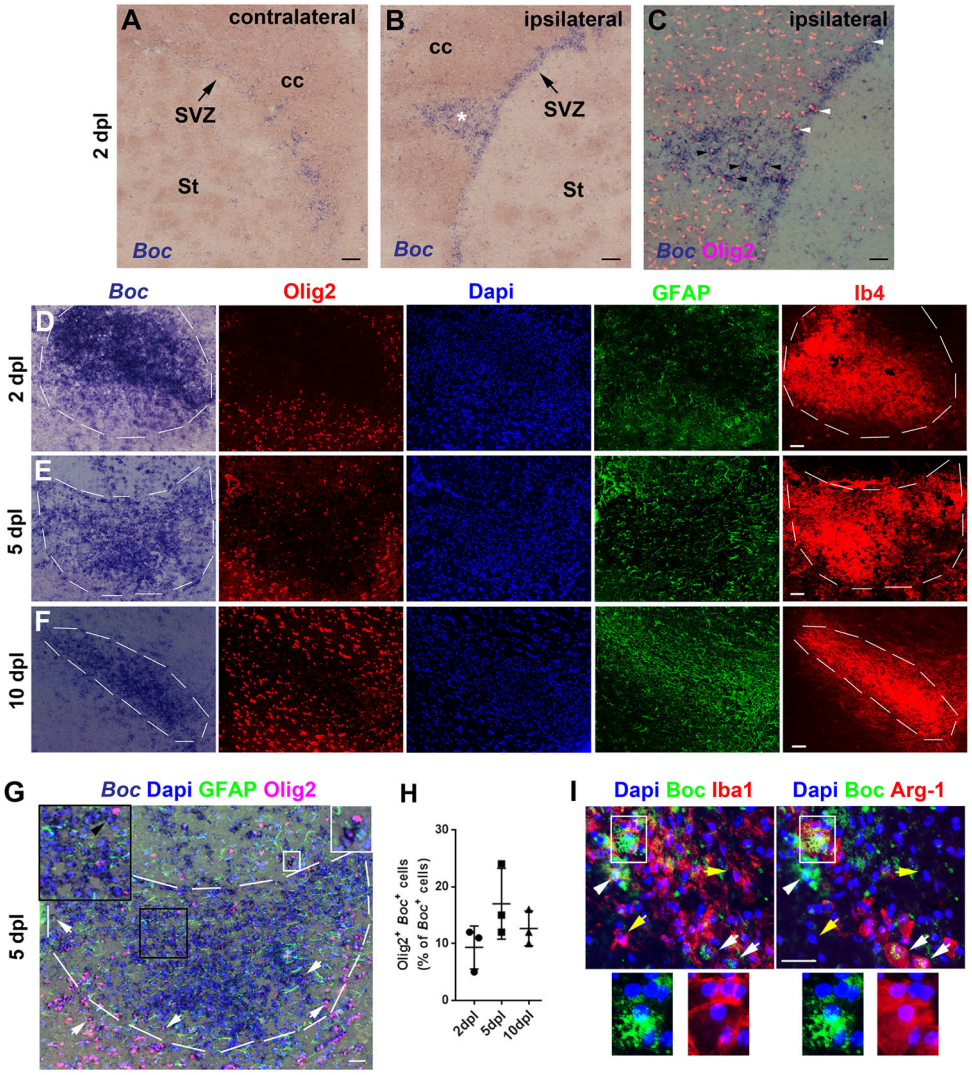

Fig. 7. Boc is highly upregulated upon focal demyelination of the corpus callosum. (A-C) *In situ* hybridization of slices derived from wild-type animals 2 days after LPC injection. *Boc* transcription is detected at a low level in the contralateral SVZ (A) and clearly upregulated in the ipsilateral side in the SVZ and the corpus callosum at a level corresponding to the LPC injection site (white star, B). (C) Immunostaining using the Olig2 antibody shows that most Olig2$^+$ cells arising from the SVZ (white arrowheads) or already recruited into the lesion (black arrowheads) co-express *Boc*. (D-F) *In situ* hybridization and double immunolabelling using the Olig2 and GFAP markers performed on the same slice derived from animals at 2 (D), 5 (E) and 10 (F) dpl. Ib4 staining was performed on the consecutive slice at each time point. The highest level of *Boc* is observed in the centre of the lesion in which Ib4$^+$ microglia and/or macrophages are the most abundant. The dashed lines outline the lesion area. (G,H) At 5 dpl, the merged images indicate the presence of *Boc*$^+$ cells co-expressing the Olig2 marker (white arrows and white box in G) and the vast majority of cells co-expressing neither Olig2 nor GFAP (black arrowhead in the black inset in G). Only a tiny number of GFAP$^+$ cell bodies colocalize with *Boc*$^+$ staining (not shown). The quantification of *Boc*$^+$ Olig2$^+$ cells is shown in H. Data are mean±s.e.m. (I) Triple immunolabelling of a brain slice derived from an animal demyelinated via LPC injection into the corpus callosum at 5 dpl. Boc signal is observed in Iba1$^+$ cells (white arrowheads) as well as in Iba1$^+$ Arg-1$^+$ (white arrows and boxed area) cells. Bottom panels are magnifications of the boxed area. The yellow arrows indicate Iba1$^+$ Boc$^-$ microglia and/or macrophages. Scale bars: 100 µm in A,B,D-F; 50 µm in C,G,I.

the SVZ towards the lesion might also be impaired in the mutant. However, the hypothesis remains to be investigated. Our previous work has shown that, in the lesion of wild-type animals, the *Gli1* effector was upregulated at a much lower level than other components of Shh signalling, such as Smo (Ferent et al., 2013). Given the decrease of *Gli1* transcription in the healthy Boc mutant mice (present work), *Gli1* upregulation was barely detectable in the lesion of the Boc mutant (data not shown). In contrast, the visualization of *Boc* transcription at 2, 5 and 10 dpl clearly indicated that a high upregulation of *Boc* was maintained throughout the repair process. The immunodetection of the oligodendroglial (Olig2$^+$) and astroglial (GFAP$^+$) cells on the same section, and microglia and/or macrophage (Ib4$^+$) on an adjacent section showed a notable similarity between the *Boc* signal and the Ib4$^+$ microglia and/or macrophage staining (Fig. 7D-F). The analysis of the merged images for *Boc*$^+$ and Olig2$^+$ cells at each time point allowed the detection of *Boc*$^+$ cells co-expressing the Olig2 marker and corresponding to a small and non-significantly different proportion (9±3, 17±4 and 13±2% for 2, 5 and 10 dpl, respectively) of all Boc$^+$ cells (Fig. 7G,H). The co-expression of Boc and GFAP was even more restricted (Fig. 7G) and thus most *Boc*$^+$ cells appeared to be neither oligodendroglial nor astroglial cells. Therefore, many *Boc*$^+$ cells could be microglia or macrophages. In order to check such hypothesis, we performed triple immunolabelling of brain slices derived from LPC-demyelinated animals at 5 dpl by using Iba1 as a global marker of microglia and/or macrophages and Arg-1 as a

Development (2019) 146, dev172502. doi:10.1242/dev.172502

marker of microglia and/or macrophages displaying pro-regenerative activity (Miron et al., 2013). The images evidenced Boc$^+$ cells expressing Iba1 alone or together with Arg-1 (Fig. 7I). Together, these results indicate that the absence of Boc prevents myelin repair by impairing OPC recruitment/differentiation, and also results in discrete morphological differences in microglia and/or macrophages that are consistent with Boc expression in this cell type.

Boc expression is required for microglia and/or macrophage transition from a highly to a faintly ramified morphology

Under healthy conditions, the so-called 'resting' microglia and/or macrophages display highly dynamic processes continuously elongating and retracting to explore the tissue environment (Nimmerjahn et al., 2005). Upon recognition of inflammatory stimuli, microglia and/or macrophages can rapidly retract their processes in order to become more ameboid and therefore efficient mobile effector cells able to fulfil local immune-related functions (Kierdorf and Prinz, 2013). The morphological differences detected for microglia and/or macrophages in the *Boc* mutant upon LPC-mediated demyelination led us to investigate whether the presence or the absence of Boc could influence the morphological transition between highly and faintly ramified cells. We took advantage of live-imaging approaches (Hristovska and Pascual, 2015) to visualize microglia and/or macrophages in the context of myelin repair in living animals. We crossed the *Boc* mutant mice with a strain expressing the YFP reporter under the promoter of the chemokine receptor CX3CR1, prominently expressed in microglia and/or macrophages (Wolf et al., 2013; Yona et al., 2013). Animals received the copper chelator cuprizone in their food for 12 weeks to induce an extensive demyelination of the cerebral cortex (Skripuletz et al., 2008; Gudi et al., 2009), as shown in Fig. 8A-C. Transcranial live-imaging of YFP$^+$ microglia and/or macrophages was carried out in the somatosensory cortex from both genotypes using two-photon microscopy. Animals were live-imaged on day 3 (D3) and day 8 (D8) after cuprizone removal from the diet while remyelination was already ongoing (Skripuletz et al., 2008; Gudi et al., 2009). On D3, microglia and/or macrophages appeared to be more ramified in *Boc* mutant mice compared with wild-type mice (Fig. 8D). Indeed, the cell processes were highly ramified in the mutant, similar to a resting phenotype, whereas they were retracted in the wild-type animals. In agreement with this observation, the quantification of processes complexity indicated a significantly higher value in *Boc* mutants compared with wild type (1.63±0.003 versus 1.57±0.013; P=0.05; Fig. 8E). Remarkably, the density of microglia and/or macrophages did not significantly differ with regards to the genotype or cuprizone treatment (Fig. 8F). Moreover, as already shown in the context of injury (Eyo et al., 2016), we visualized spontaneous focal events (SFE) corresponding to the attraction of microglia and/or macrophage processes within minutes at a focal point, followed by the subsequent invasion of the area by

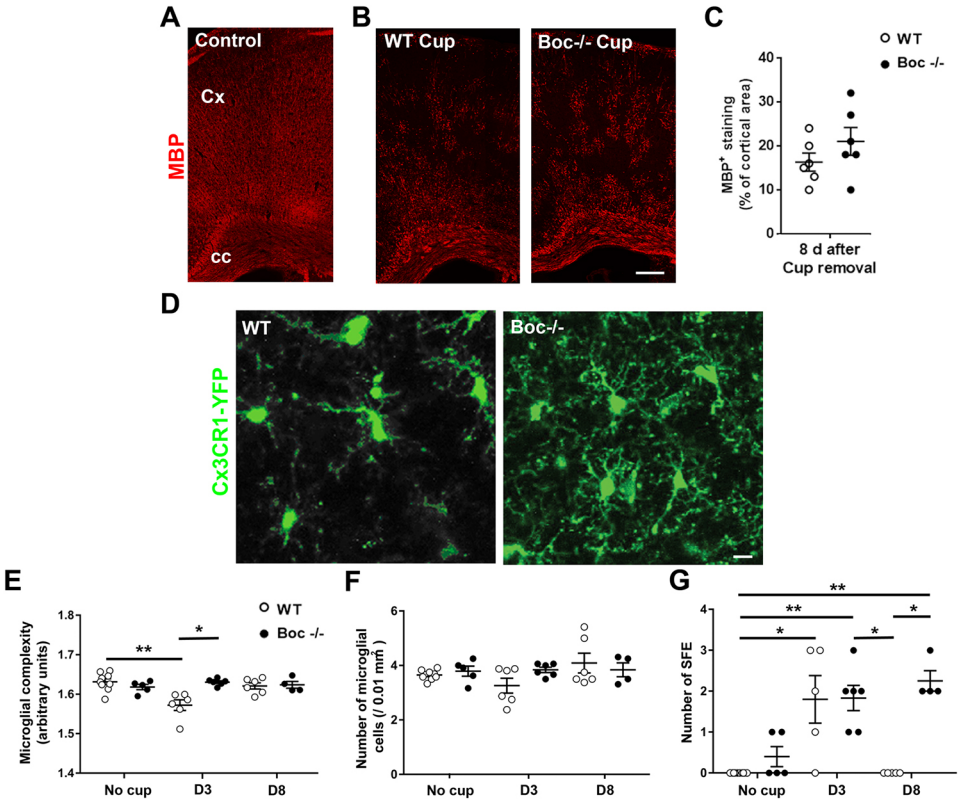

Fig. 8. Microglia and/or macrophages fail to switch from a resting-like to an activated-like state in the demyelinated cerebral cortex of the Boc mutant mice. (A) MBP immunostaining in the dorsal forebrain of a wild-type mouse (control). (B) MBP staining in wild-type and Boc mutant animals fed with cuprizone-supplemented (Cup) chow for 12 weeks and analysed 8 days after cuprizone removal. (C) Comparable levels of MBP immunofluorescence are observed, reflecting a similar extent of demyelination at this early time point after cuprizone removal. (D) Live images of CX3CR1-YFP microglia and/or macrophages in the cerebral cortex of wild-type and Boc mutant mice 3 days after cuprizone removal. (E,F) Quantification of the complexity of microglia and/or macrophages shows their inability to display the activated morphology observed for the wild-type cells 3 days after cuprizone removal (E). In contrast, the densities of cells are not significantly different under any conditions (F). (G) Quantification of the number of spontaneous focal events shows that, in the mutant, microglia and/or macrophage processes remain attracted towards focal events. Scale bars: 200 µm in B; 10 µm in D. Statistical analysis used Kruskal-Wallis and Dunn's multiple comparison test (E-G). *P<0.05; **P<0.01. Data are mean±s.e.m.

Development (2019) 146, dev172502. doi:10.1242/dev.172502

those processes (Movie 1). As expected, SFE could be detected in the cuprizone-treated wild-type and *Boc* mutant mice at D3. However, although SFE completely disappeared in the wild-type animals at D8, indicating a significant recovery, they were still detected in *Boc* mutants at this time point (P=0.05; Fig. 8G). Remarkably, in *Boc* mutant mice receiving a regular diet, some SFE could be detected, whereas they were completely absent from their wild-type counterparts. Together, these results indicate that, during myelin repair, *Boc* inactivation is associated with morphological differences in microglia and/or macrophages that mimic the transition between a 'resting-like' and an 'activated-like' state. In addition, *Boc* mutant mice display impaired responses in demyelinating conditions.

DISCUSSION

The investigation of *Boc* mutants performed in the present work provides evidence for the involvement of Boc in both developmental and repairing myelination. The first phenotypic feature observed in *Boc* mutants was the transient decrease in OPC production related to a reduced number of $Sox2^+$ neural progenitors and the decreased capacity of OPCs to proliferate. Together with the inability of *Boc* mutant glial cells to upregulate *Gli1 in vitro*, these data support the hypothesis that Boc may be positively involved in Shh-mediated dorsal oligodendrogenesis. Although questioned for a long time (Kessaris et al., 2006), Shh involvement in this process was recently demonstrated. Indeed, the neural progenitors located in the dorsal germinative zone of the forebrain are Shh-responding cells (Ahn and Joyner, 2005), which proliferate in a Shh-dependent manner (Balordi and Fishell, 2007) and give rise to oligodendroglial lineage cells at the neonatal period (Tong et al., 2015; Sanchez and Armstrong, 2018). However, whereas the conditional inactivation of the key transducer of Shh signalling, Smo, leads to a persistent oligodendrocyte decrease (Tong et al., 2015), *Boc* mutant mice display a rapid recovery of oligodendrocyte density. To account for this discrepancy, a first hypothesis relies on the existence of partially redundant functions of Boc with other Shh co-receptors, including Cdo and Gas1 as previously proposed in Shh-mediated proliferation of cerebellar progenitors (Izzi et al., 2011). This hypothesis is nevertheless unlikely because, if Cdo and/or Gas1 had redundant functions with Boc, the Boc-deficient glial cells should have upregulated *Gli1* in response to exogenous Shh. However, our data indicate no *Gli1* upregulation *in vitro*. Moreover, *Gli1* transcription is clearly downregulated in the early postnatal dorsal forebrain of the x*Boc* mutant. On the other hand, the recent report that Cdo promotes oligodendrocyte differentiation and myelination *in vitro* (Wang and Almazan, 2016) is not in support of a putative role for Cdo in oligodendroglial proliferation. A more plausible hypothesis could be the existence of compensatory mechanisms mediated by one of the other potent positive regulators of dorsal OPC production, such as Wnt or FGF (Azim et al., 2012, 2014, 2016; Ortega et al., 2013). If so, the absence of compensation observed upon conditional inactivation of *Smo* could be related to the experimental approach, based on the administration of an adenoviral vector at birth, which probably induced a massive and abrupt drop in oligodendrogenesis that may conceivably be more difficult to be compensated for.

Contrasting with its limited expression in cells of the oligodendroglial lineage, the wide expression of Boc in neurons is in support of a major neuronal function susceptible to indirectly influence myelination. In agreement with this hypothesis, Boc has initially been characterized as a member of the family of membrane-bound cell-adhesion molecules that provide axon-derived instructive cues for myelination (Emery, 2010; Hughes and Appel, 2016; Klingseisen and Lyons, 2018). Therefore, we tested the Src-family tyrosine kinase (SFK) Fyn (data not shown) as the most well-known integrator of neuronal signals during active myelination and notably for its role in the site-specific translation of MBP (White et al., 2008; White and Kramer-Albers, 2014). Although we were unable to detect any modification in SFK phosphorylation that might support the involvement of neuronal Boc-mediated signals in the spatiotemporal regulation of MBP production, we cannot exclude the possibility that Boc may mediate such a signal via a signalling cascade different from Fyn. However, our work importantly shows that the absence of functional Boc results in a clear reduction in the calibre of callosal axons and in a significant decrease in the neurofilament NF-M. The former observation is able to account for the persistence of a lower production of MBP given that small calibre axons require less MBP for their ensheathment by myelin. The latter deserves to be considered in the molecular mechanism possibly contributing to the defective radial growth of callosal axons. Remarkably, the decrease in NF-M is consistent with the role of Boc in neurite outgrowth previously reported in cultures of cortical neural progenitor cells. Indeed, the induction of Boc expression in those cells was found to specifically induce a high NF-M expression (Vuong et al., 2017). The role of NF-M in the radial growth of both large (>2 µm) and small (<2 µm) classes of myelinated fibres has been thoroughly investigated mainly in the peripheral nervous system where this process is necessary for the rapid impulse transmission in axons with a diameter over 1 µm (Eyer and Peterson, 1994; Garcia et al., 2003; Barry et al., 2012; Yuan and Nixon, 2016). Therefore, although further work is required to demonstrate a potential link between the altered radial growth of the callosal axons and the decreased expression of the neurofilament NF-M, both phenotypic features are likely to impair the fine tuning of postnatal active myelination in the absence of functional Boc.

In the context of demyelination, the Boc phenotype on cells of the oligodendroglial lineage is reminiscent of the phenotype previously reported when Shh signalling is inhibited (Ferent et al., 2013), as shown by the delay of OPC recruitment into the lesion, the decrease in the proliferation of these cells and the defect in their differentiation into immature oligodendrocytes. In contrast, *Boc* mutants do not phenocopy Shh signalling blockade at the level of astrocytes, microglia and/or macrophages (Ferent et al., 2013) because those cells were not increased in the *Boc* mutants. Moreover, the fact that the mutant fails to reach the level of myelin regeneration observed in the control animals was surprising given the apparent inability of Boc to regulate OPC differentiation during development. However, the unexpected consequences of non-functional Boc on microglia and/or macrophages provide an answer to these discordant observations. The high upregulation of Boc in an area encompassing the region populated by activated microglia and/or macrophages, most importantly the colocalization of Boc with one of the markers of pro-regenerative microglia and/or macrophages, as well as the inability of the mutant microglia and/or macrophages to retract their processes both support the hypothesis that OPC differentiation failure in the mutant may likely be related to defective microglia and/or macrophage activation. Consistently, during the past few years, a plethora of evidence have highlighted the pro-remyelination roles of microglia and/or macrophages, notably in the clearance of myelin debris, the secretion of growth factors or the remodelling of the extracellular matrix in myelin repair (Lloyd et al., 2017). Therefore, it is conceivable that the behavioural anomalies of microglia and/or macrophages observed in *Boc*

Development (2019) 146, dev172502. doi:10.1242/dev.172502

mutants disturb the ability of these cells to play their pro-remyelinating role, by altering microglia and/or macrophage reactive state (Kotter et al., 2006; Miron et al., 2013; Orihuela et al., 2016; Ransohoff, 2016; Church et al., 2017). Moreover, the recent observation that the dynamic state of the actin cytoskeleton profoundly affects microglia and/or macrophage behaviour (Uhlemann et al., 2016) might open the way to further investigations regarding a potential relationship between Boc and cell cytoskeletal dynamics in microglia and/or macrophages.

The recent identification of *Boc* variants in individuals with holoprosencephaly and the characterization of *Boc* as a modifier locus in this pathology, which is the most common malformation of the forebrain in humans, pinpoint Boc as a new therapeutic target (Roessler and Muenke, 2010; Hong et al., 2017). Given the accurate tuning of CNS myelination according to a precise spatiotemporal pattern, which coincides with the appearance of cognitive and behavioural functions (Nagy et al., 2004; Fields, 2008; Dean et al., 2016; Poggi et al., 2016), the delayed myelination, together with the reduction in axon calibre, may likely be associated with potential cortical dysfunctions in the absence of functional Boc. Moreover, Boc variants in individuals presenting with a demyelinating disease should be considered in the therapeutic strategy used, in particular when the Shh pathway is known to contribute to the remyelinating effects of the selected treatment, as recently shown for the drug Fingolimod (Zhang et al., 2015).

MATERIALS AND METHODS

Animals

The *Boc* knockout mouse strain (Okada et al., 2006) was obtained and maintained on a C57BL/6 background. The mouse strain *CX3CR1tm2.1(Cre/ERT2)* (thereafter called *CX3CR1^{CreER}-YFP*) expressing the YFP reporter under the promoter of the chemokine receptor CX3CR1 (Wolf et al., 2013; Yona et al., 2013) was provided by the Jackson Laboratory. Surgeries and perfusions were performed under ketamine (100 mg/kg)/xylazine (10 mg/kg)-induced anaesthesia. Two-month-old male animals were used unless otherwise indicated. The number of animals is indicated in each graph as the data obtained for each animal are shown. All animal studies were carried out according to the guidelines established by the European Communities Council Directive (86/806/EEC) for the care and use of laboratory animals. All experimental and surgical protocols were approved by the Regional Ethics Committee CEEA26, Ministère de L'Education Nationale, de l'Enseignement Supérieur et de la Recherche. Animals were housed under standard conditions with access to water and food *ad libitum* on a normal 12 h light/dark cycle.

LPC-induced focal demyelination

The lysolecithin (LPC)-induced demyelination was carried out as previously described (Ferent et al., 2013). The injection was performed at the following coordinates (to the bregma): anteroposterior (AP) +1 mm, lateral +1 mm, dorsoventral (DV) −2.2 mm. Mice were sacrificed at different survival time points: 2, 5, 10, 15, 21 and 30 days postlesion (dpl). The brain was removed, frozen in liquid nitrogen and cryostat sections (14 µm) were cut.

Cuprizone-induced demyelination

Boc$^{-/-}$;CX3CR1^{CreER}-YFP male animals were placed on a diet containing 0.2% cuprizone (Sigma-Aldrich) mixed into powdered food. The food was available *ad libitum* for 12 weeks and replaced every 2 days.

Primary glial cell cultures

Primary glial cell cultures were prepared from postnatal day (P) 1-2 mouse dorsal forebrain derived from each genotype as previously described (Feutz et al., 2001). Cultures containing astrocytes, oligodendrocytes and microglia cells were then incubated in 5% CO_2 and 95% air in a humidified atmosphere (90%) at 37°C. After 5 DIV, the medium was replaced by fresh medium supplemented or not with the recombinant Shh protein [4 nM; Shh (C24II) N-Terminus, BioTechne; 4 nM] or SAG (DC Chemicals; 3×10^{-7} M) which was renewed at 7 DIV. At 9 DIV, the cells were either collected in Trizol reagent for RNA extraction and quantitative RT-PCR analysis or incubated for 2 h with BrdU (3 µg/ml) before PFA 4% fixation for immunocytofluorescence. For enriched oligodendrocyte cultures, shaking of the flasks containing the primary mixed glial cells was carried out at 9 DIV in order to detach the oligodendroglial cells that were further cultured for 3 or 5 additional DIV in an oligodendrocyte medium as described previously (O'Meara et al., 2011). The number of independent cultures is indicated in each graph in which the data obtained from each culture is individually represented.

Histological procedures

The animals were deeply anesthetized before perfusion with 4% paraformaldehyde (PFA). Brains were post-fixed in 4% PFA for 4 h and incubated overnight in a 30% sucrose solution. Hemispheres were then frozen into a Shandon Cryomatrix and stored at −80°C before performing cryostat sections (14 µm). For immunohistochemistry the primary antibodies were as follows: anti-Boc (goat polyclonal, R&D, AF2385, 1:100; Izzi et al., 2011), anti-NeuN (mouse monoclonal, Millipore, MAB377, 1:500; Ferent et al., 2014), anti-Sox2 (goat polyclonal, Santa Cruz, sc-17320, 1:500), anti-Olig2 (rabbit polyclonal, Millipore, AB9610, 1:500; mouse monoclonal, Millipore, MABN50, 1:200; Ferent et al., 2013), anti-PDGFRa (rat; BD Pharmingen, 558774, 1:500; Ferent et al., 2013), anti-myelin basic protein (MBP) (rabbit polyclonal, Millipore, AB980, 1:500; Ferent et al., 2013), anti-adenomatus polyposis coli (APC/CC1) (mouse monoclonal, Calbiochem, OP80, 1:250; Ferent et al., 2013), anti-Ki67 (mouse monoclonal; BD Pharmingen, 550609, 1:100; Ferent et al., 2013), anti-BrdU antibody (rat monoclonal, Abcam, Ab6326, 1:250; Ferent et al., 2013), anti-glial fibrillary acidic protein (GFAP) (rabbit polyclonal, Dako, ZO334, 1:1000; mouse monoclonal, Sigma-Aldrich, G3893, 1:1000; Ferent et al., 2013), Iba1 (rabbit, Wako, W1W019-19741, 1:250), isolectin GS-IB4 conjugated to Alexa Fluor 568 (Thermo Fisher Scientific, I21412, 1:250; Ferent et al., 2013), arginase 1 (goat, Santa-Cruz, sc-18355, 1:100), CNPase (mouse, Sigma-Aldrich, 11-5B, 1:500), PLP (mouse, Millipore, Mab388, 1:250). The secondary antibodies were: donkey anti-goat Alexa 488, anti-mouse 647 and anti-rabbit 546 (Thermo Fisher Scientific, A11055, 1:250; A31571, 1:750; A10040, 1:250); goat anti-rabbit cyanine 3 conjugated (Jackson Immunoresearch, 111-165-003, 1:250); goat anti-mouse Alexa 488 and anti-rabbit Alexa 633 (Thermo Fisher Scientific, A11026, 1:250 and A21070, 1:750).

In situ hybridization experiments were performed as previously described (Ferent et al., 2013). The *Boc* riboprobe was kindly provided by Dr R.S. Krauss (Mount Sinai, New York, USA).

Image acquisition and analysis

Images were taken using the microscope analysing system Axiovision 4.2 (Carl Zeiss), the confocal Zeiss LSM 510-Meta Confocor 2, Leica TCS SP8 with LAS AF software and slide scanner Model Panoramic 250 Flash II 3DHISTECH with CaseViewer software. Analyses were performed using ImageJ software. Immunofluorescent-positive cells were counted in one sitting for every other five sections throughout the whole demyelinated lesion per mouse and averaged for each animal. Cell counts are the results from at least three animals (the exact number is indicated in each graph) or three independent cultures and are expressed per surface unit. Alternatively, the area occupied by marker immunofluorescence is expressed as percentage of the studied area. The lesion surface was determined by measuring the area of the nuclear densification or the absence of small cell chains (correlated with myelin loss visualized by MBP staining) on every other five slices throughout the whole demyelinated lesion per mouse.

Electron microscopy

Three 12-week-old male mice per genotype were perfused with 2% PFA and 2% glutaraldehyde. Ultrathin slices of resin-embedded osmium post-fixed corpus callosum (related to the genu part) were examined using a transmission electron microscope (1011 JEOL) equipped with a Gatan digital camera. The g ratio (the ratio between the axon diameter and fibre diameter corresponding to myelin sheath+axon diameter) was estimated by measuring the minimum and maximum axon diameter and fibre diameter for each axon using ImageJ software. At least 50 randomly chosen myelinated axons were evaluated for each animal.

Development (2019) 146, dev172502. doi:10.1242/dev.172502

RT-qPCR analysis

Three animals per group were sacrificed by decapitation. Brains were dissected and frozen in liquid nitrogen for further processing. Total RNA was isolated by using the Trizol Technique (Thermo Fisher Scientific) and RNeasy Mini Kit (Qiagen). For the primary glial cell cultures, the cells were directly collected in Trizol reagent. Reverse transcription was performed using the High Capacity cDNA Reverse Transcription kit (Applied Biosystems). Quantitative real-time PCR was carried out by using the Power SYBR-Green Master mix (Applied Biosystems) and gene expression was analysed with the 7300 Systems SDS Software (Applied Biosystems) normalized to reference genes GAPDH. The primers used were as follows: GAPDH fwd, 5′-GTCGGTGTGAACGGATTTGG-3′; GAPDH rev, 5′-GACTCCACGACATACTCAGC-3′; Olig2 fwd, 5′-GCAGCGAGCACCTCAAATCT-3′; Olig2 rev, 5′-GGGATGATCTAAGCTCTCGAATG-3′; Gli1 fwd, 5′-ACAAGTGCACGTTTGAAGGCTGTC-3′; Gli rev, 5′-GCTGCAACCTTCTTGCTCACACAT-3′.

Western blotting

Tissues were homogenized in cold RIPA lysis buffer (Biorad) in the presence of protease inhibitors (Sigma-Aldrich). The protein extract concentration was measured using the BCA method (Thermo Fisher Scientific). Proteins (30 µg) were separated using a 12% polyacrylamide gel followed by blotting onto a PVDF membrane using the trans-blot Turbo Transfer Pack (Biorad). Blots were incubated with the following antibodies: anti-MBP (rabbit, Millipore, Mab386), anti-gelsolin (rabbit, Abcam; Zuchero et al., 2015), anti-NF-M (mouse, Abcam, Ab7794) and anti-β-actin (mouse, Sigma-Aldrich; Ferent et al., 2014). Goat anti-mouse- and anti-rabbit Dylight-conjugated secondary antibodies were used (Thermo Fisher Scientific) and membranes were scanned with the Odyssey InfraRed Scanner (Li-Cor). Bands of interest were quantified by measuring their integrated intensities using the Odyssey software V3.0. Alternatively, goat anti-rabbit or anti-mouse horseradish peroxydase (Biorad) were used and immunoreactivity was revealed with enhanced chemiluminescence. The membranes were exposed to the chemiluminescent substrate Radiance Plus (Biorad) according to the manufacturer's instructions and then quantified using the Bio-Rad ChemiDoc MP Imaging System (Biorad). The densitometric values were systematically normalized to β-actin expression.

Two-photon *in vivo* imaging

For transcranial imaging, we performed thin-skull window preparation over the somatosensory cortex. Briefly, mice were deeply anesthetized with isoflurane (3-4%, Isovet, Piramal Healthcare) and mounted in a stereotaxic apparatus (D. Kopf Instruments). Carprofen (5 mg/kg s.c.) was injected at the beginning of the surgery to diminish post-surgical pain and inflammation. After the skull was exposed, a thin custom-made metal implant was glued, allowing delimitation of the area over the somatosensory cortex. The skull was then carefully thinned using a high-speed dental drill. To avoid heat-induced damage, we repeatedly interrupted drilling and applied cold sterile saline. When a 20 to 30 µm skull thickness was reached, we applied a thin layer of cyanoacrylate glue and placed a cover glass on top of the thinned skull. Mice were imaged on the 2nd and 7th post-operatory days, which are respectively the 3rd and 8th day of the end of cuprizone treatment. These two time points represent early remyelination and a more advanced remyelination. For each imaging session, mice were anesthetized with a mixture of ketamine (100 mg/kg) and xylazine (10 mg/kg), and their body temperature was maintained at 37°C. Imaging was performed using a two-photon microscope (Olympus) with a Ti:Sapphire laser (Mai-Tai, Spectra-Physics) tuned to 940 nm. We used a 20× water-immersion objective (0.95 N.A. Olympus) to acquire images and maintained the laser power below 30 mW. Fluorescence was detected using a 560 nm dichroic mirror coupled to a 525/50 nm emission filter and a photomultiplier tube in whole-field detection mode. We imaged microglia and/or macrophages at a depth of 50-150 µm. Every 30 s we acquired 30-35 consecutive stack images with a step size of 1 µm/optical section over an area of 200×200 µm and a resolution of 521×521 pixels. Recordings generally lasted 10-15 min (20-30 stacks).

Live imaging analysis

Image processing and analysis were performed using custom-written program under MatLab and ImageJ software. Regions of interest containing the totality of one microglia and/or one macrophage were delimited manually. Brightness/contrast and drift correction in x, y and z planes of images were adjusted by an automated post-processing. Drift correction was performed by registering each volume to a reference volume (the first volume) using shift estimation from the cross-correlation peak by FFT (fast Fourier transform). After realignment, 2D time-lapse movies were generated from standard deviation intensity projections of z-stacks. To quantitatively measure cell complexity, the images were first converted into binary. The cell complexity index was obtained by assessing the fractal dimension of the cell by calculating the Hausdorff dimension using a custom-written MatLab program. For each cell, the cell complexity index corresponded to the complexity value obtained at the beginning of the recording (t0). We identified spontaneous microglia and/or macrophage process convergence as events during which processes from one or (more frequently) several cells converged toward a focal point. All observed spontaneous microglia and/or macrophage process convergence events, regardless of size, were manually counted in a 200×200×30 µm visual field from all our recordings. Microglia and/or macrophage density was manually counted by marking each cell body in the visual field. The total number of microglia and/or macrophages was then divided to generate a measure of cell density for 10^4 µm^2.

Statistical analysis

Size sample was defined on the basis of our previous experiments. For cell counts, the mean number of immunopositive cells was evaluated per image area to determine the density of cells/surface area. Mice were allocated into experimental groups based on their genotype. Data analysis was carried out blind to the genotype of the mice. Data are expressed as mean±s.e.m. Statistical analysis was performed with GraphPad Prism 7.0 software. The significance of differences between means was evaluated using Student's unpaired t-test for two independent group comparisons and ANOVA followed by ad hoc post-tests for comparisons of more than two groups and/or several variables. In case of absence of distribution normality, non-parametric tests (Mann–Whitney, Kruskal-Wallis) were used. Appropriate corrections were carried out according to the determination of the variance of each sample. Dixon's Q test was used to identify potential outliers. Significance of $P<0.05$ was used for all analyses.

Acknowledgements

We thank Prof. Dr Leda Dimou for preliminary discussions regarding this work, Olivier Trassard and Alain Schmitt for technical assistance in imaging and transmission electron microscopy, respectively.

Competing interests

The authors declare no competing or financial interests.

Author contributions

Conceptualization: J.F., E.T.; Methodology: M.Z., J.F., I.H., Y.L., A.Z., A.K., O.P., E.T.; Validation: O.P., E.T.; Formal analysis: M.Z., I.H., Y.L., O.P., E.T.; Investigation: M.Z., J.F., I.H., Y.L., A.Z., A.K., M.-E.M.; Data curation: O.P., E.T.; Writing - original draft: E.T.; Writing - review & editing: J.F., O.P., F.C., E.T.; Visualization: M.Z., I.H., Y.L., A.Z., A.K.; Supervision: E.T.; Project administration: E.T.; Funding acquisition: E.T.

Funding

This work was supported by the Fondation pour l'Aide à la Recherche sur la Sclérose en Plaques (RAK14147LLA and RAK17128LLA to E.T.) and the Agence Nationale de la Recherche (RPV15198LLA to E.T.). M.Z. was the recipient of a PhD student fellowship from the Ministère de l'Enseignement Supérieur et de la Recherche.

Supplementary information

Supplementary information available online at
http://dev.biologists.org/lookup/doi/10.1242/dev.172502.supplemental

References

Ahn, S. and Joyner, A. L. (2005). In vivo analysis of quiescent adult neural stem cells responding to Sonic hedgehog. *Nature* **437**, 894-897. doi:10.1038/nature03994

Allen, B. L., Song, J. Y., Izzi, L., Althaus, I. W., Kang, J.-S., Charron, F., Krauss, R. S. and McMahon, A. P. (2011). Overlapping roles and collective requirement for the coreceptors GAS1, CDO, and BOC in SHH pathway function. *Dev. Cell* **20**, 775-787. doi:10.1016/j.devcel.2011.04.018

Azim, K., Raineteau, O. and Butt, A. M. (2012). Intraventricular injection of FGF-2 promotes generation of oligodendrocyte-lineage cells in the postnatal and adult forebrain. *Glia* **60**, 1977-1990. doi:10.1002/glia.22413

Azim, K., Rivera, A., Raineteau, O. and Butt, A. M. (2014). GSK3beta regulates oligodendrogenesis in the dorsal microdomain of the subventricular zone via Wnt-beta-catenin signaling. *Glia* **62**, 778-779. doi:10.1002/glia.22641

Azim, K., Berninger, B. and Raineteau, O. (2016). Mosaic subventricular origins of forebrain oligodendrogenesis. *Front. Neurosci.* **10**, 107. doi:10.3389/fnins.2016.00107

Balordi, F. and Fishell, G. (2007). Hedgehog signaling in the subventricular zone is required for both the maintenance of stem cells and the migration of newborn neurons. *J. Neurosci.* **27**, 5936-5947. doi:10.1523/JNEUROSCI.1040-07.2007

Barry, D. M., Stevenson, W., Bober, B. G., Wiese, P. J., Dale, J. M., Barry, G. S., Byers, N. S., Strope, J. D., Chang, R., Schulz, D. J. et al. (2012). Expansion of neurofilament medium C terminus increases axonal diameter independent of increases in conduction velocity or myelin thickness. *J. Neurosci.* **32**, 6209-6219. doi:10.1523/JNEUROSCI.0647-12.2012

Church, J. S., Milich, L. M., Lerch, J. K., Popovich, P. G. and McTigue, D. M. (2017). E6020, a synthetic TLR4 agonist, accelerates myelin debris clearance, Schwann cell infiltration, and remyelination in the rat spinal cord. *Glia* **65**, 883-899. doi:10.1002/glia.23132

Dai, J., Bercury, K. K., Ahrendsen, J. T. and Macklin, W. B. (2015). Olig1 function is required for oligodendrocyte differentiation in the mouse brain. *J. Neurosci.* **35**, 4386-4402. doi:10.1523/JNEUROSCI.4962-14.2015

Dean, D. C., III, O'Muircheartaigh, J., Dirks, H., Travers, B. G., Adluru, N., Alexander, A. L. and Deoni, S. C. (2016). Mapping an index of the myelin g-ratio in infants using magnetic resonance imaging. *Neuroimage* **132**: 225-237. doi:10.1016/j.neuroimage.2016.02.040

Ellis, P., Fagan, B. M., Magness, S. T., Hutton, S., Taranova, O., Hayashi, S., McMahon, A., Rao, M. and Pevny, L. (2004). SOX2, a persistent marker for multipotential neural stem cells derived from embryonic stem cells, the embryo or the adult. *Dev. Neurosci.* **26**, 148-165. doi:10.1159/000082134

Emery, B. (2010). Regulation of oligodendrocyte differentiation and myelination. *Science* **330**, 779-782. doi:10.1126/science.1190927

Eyer, J. and Peterson, A. (1994). Neurofilament-deficient axons and perikaryal aggregates in viable transgenic mice expressing a neurofilament-beta-galactosidase fusion protein. *Neuron* **12**, 389-405. doi:10.1016/0896-6273(94)90280-1

Eyo, U. B., Peng, J., Murugan, M., Mo, M., Lalani, A., Xie, P., Xu, P., Margolis, D. J. and Wu, L. J. (2016). Regulation of physical microglia-neuron interactions by fractalkine signaling after status epilepticus. *eNeuro* **3**, 1-14. ENEURO.0209-16.2016. doi:10.1523/ENEURO.0209-16.2016

Fabre, P. J., Shimogori, T. and Charron, F. (2010). Segregation of ipsilateral retinal ganglion cell axons at the optic chiasm requires the Shh receptor Boc. *J. Neurosci.* **30**, 266-275. doi:10.1523/JNEUROSCI.3778-09.2010

Ferent, J., Zimmer, C., Durbec, P., Ruat, M. and Traiffort, E. (2013). Sonic Hedgehog signaling is a positive oligodendrocyte regulator during demyelination. *J. Neurosci.* **33**, 1759-1772. doi:10.1523/JNEUROSCI.3334-12.2013

Ferent, J., Cochard, L., Faure, H., Taddei, M., Hahn, H., Ruat, M. and Traiffort, E. (2014). Genetic activation of Hedgehog signaling unbalances the rate of neural stem cell renewal by increasing symmetric divisions. *Stem Cell Rep.* **3**, 312-323. doi:10.1016/j.stemcr.2014.05.016

Feutz, A. C., Pham-Dinh, D., Allinquant, B., Miehe, M. and Ghandour, M. S. (2001). An immortalized jimpy oligodendrocyte cell line: defects in cell cycle and cAMP pathway. *Glia* **34**, 241-252. doi:10.1002/glia.1058

Fields, R. D. (2008). White matter in learning, cognition and psychiatric disorders. *Trends Neurosci.* **31**, 361-370. doi:10.1016/j.tins.2008.04.001

Franklin, R. J. M. and Ffrench-Constant, C. (2017). Regenerating CNS myelin - from mechanisms to experimental medicines. *Nat. Rev. Neurosci.* **18**, 753-769. doi:10.1038/nrn.2017.136

Garcia, M. L., Lobsiger, C. S., Shah, S. B., Deerinck, T. J., Crum, J., Young, D., Ward, C. M., Crawford, T. O., Gotow, T., Uchiyama, Y. et al. (2003). NF-M is an essential target for the myelin-directed "outside-in" signaling cascade that mediates radial axonal growth. *J. Cell Biol.* **163**, 1011-1020. doi:10.1083/jcb.200308159

Gibson, E. M., Purger, D., Mount, C. W., Goldstein, A. K., Lin, G. L., Wood, L. S., Inema, I., Miller, S. E., Bieri, G., Zuchero, J. B. et al. (2014). Neuronal activity promotes oligodendrogenesis and adaptive myelination in the mammalian brain. *Science* **344**, 1252304. doi:10.1126/science.1252304

Gudi, V., Moharregh-Khiabani, D., Skripuletz, T., Koutsoudaki, P. N., Kotsiari, A., Skuljec, J., Trebst, C. and Stangel, M. (2009). Regional differences between grey and white matter in cuprizone induced demyelination. *Brain Res.* **1283**, 127-138. doi:10.1016/j.brainres.2009.06.005

Harwell, C. C., Parker, P. R. L., Gee, S. M., Okada, A., McConnell, S. K., Kreitzer, A. C. and Kriegstein, A. R. (2012). Sonic hedgehog expression in corticofugal projection neurons directs cortical microcircuit formation. *Neuron* **73**, 1116-1126. doi:10.1016/j.neuron.2012.02.009

Hildebrand, C., Remahl, S., Persson, H. and Bjartmar, C. (1993). Myelinated nerve fibres in the CNS. *Prog. Neurobiol.* **40**, 319-384. doi:10.1016/0301-0082(93)90015-K

Hong, M., Srivastava, K., Kim, S., Allen, B. L., Leahy, D. J., Hu, P., Roessler, E., Krauss, R. S. and Muenke, M. (2017). BOC is a modifier gene in holoprosencephaly. *Hum. Mutat.* **38**, 1464-1470. doi:10.1002/humu.23286

Hristovska, I. and Pascual, O. (2015). Deciphering resting microglial morphology and process motility from a synaptic prospect. *Front. Integr. Neurosci.* **9**, 73. doi:10.3389/fnint.2015.00073

Hughes, E. G. and Appel, B. (2016). The cell biology of CNS myelination. *Curr. Opin. Neurobiol.* **39**, 93-100. doi:10.1016/j.conb.2016.04.013

Izzi, L., Lévesque, M., Morin, S., Laniel, D., Wilkes, B. C., Mille, F., Krauss, R. S., McMahon, A. P., Allen, B. L. and Charron, F. (2011). Boc and Gas1 each form distinct Shh receptor complexes with Ptch1 and are required for Shh-mediated cell proliferation. *Dev. Cell* **20**, 788-801. doi:10.1016/j.devcel.2011.04.017

Kang, J.-S., Mulieri, P. J., Hu, Y., Taliana, L. and Krauss, R. S. (2002). BOC, an Ig superfamily member, associates with CDO to positively regulate myogenic differentiation. *EMBO J.* **21**, 114-124. doi:10.1093/emboj/21.1.114

Kessaris, N., Fogarty, M., Iannarelli, P., Grist, M., Wegner, M. and Richardson, W. D. (2006). Competing waves of oligodendrocytes in the forebrain and postnatal elimination of an embryonic lineage. *Nat. Neurosci.* **9**, 173-179. doi:10.1038/nn1620

Kierdorf, K. and Prinz, M. (2013). Factors regulating microglia activation. *Front. Cell Neurosci.* **7**, 44. doi:10.3389/fncel.2013.00044

Kim, W. R., Chun, S. K., Kim, T. W., Kim, H., Ono, K., Takebayashi, H., Ikenaka, K., Oppenheim, R. W. and Sun, W. (2011). Evidence for the spontaneous production but massive programmed cell death of new neurons in the subcallosal zone of the postnatal mouse brain. *Eur. J. Neurosci.* **33**, 599-611. doi:10.1111/j.1460-9568.2010.07557.x

Klingseisen, A. and Lyons, D. A. (2018). Axonal regulation of central nervous system myelination: structure and function. *Neuroscientist* **24**, 7-21. doi:10.1177/1073858417703030

Kotter, M. R., Li, W. W., Zhao, C. and Franklin, R. J. (2006). Myelin impairs CNS remyelination by inhibiting oligodendrocyte precursor cell differentiation. *J. Neurosci.* **26**, 328-332. doi:10.1523/JNEUROSCI.2615-05.2006

Lloyd, A. F., Davies, C. L. and Miron, V. E. (2017). Microglia: origins, homeostasis, and roles in myelin repair. *Curr. Opin. Neurobiol.* **47**, 113-120. doi:10.1016/j.conb.2017.10.001

Lopez Juarez, A., He, D. and Richard Lu, Q. (2016). Oligodendrocyte progenitor programming and reprogramming: toward myelin regeneration. *Brain Res.* **1638**, 209-220. doi:10.1016/j.brainres.2015.10.051

McKenzie, I. A., Ohayon, D., Li, H., de Faria, J. P., Emery, B., Tohyama, K. and Richardson, W. D. (2014). Motor skill learning requires active central myelination. *Science* **346**, 318-322. doi:10.1126/science.1254960

Menn, B., Garcia-Verdugo, J. M., Yaschine, C., Gonzalez-Perez, O., Rowitch, D. and Alvarez-Buylla, A. (2006). Origin of oligodendrocytes in the subventricular zone of the adult brain. *J. Neurosci.* **26**, 7907-7918. doi:10.1523/JNEUROSCI.1299-06.2006

Miron, V. E., Boyd, A., Zhao, J. W., Yuen, T. J., Ruckh, J. M., Shadrach, J. L., van Wijngaarden, P., Wagers, A. J., Williams, A., Franklin, R. J. et al. (2013). M2 microglia and macrophages drive oligodendrocyte differentiation during CNS remyelination. *Nat. Neurosci.* **16**, 1211-1218. doi:10.1038/nn.3469

Nagy, Z., Westerberg, H. and Klingberg, T. (2004). Maturation of white matter is associated with the development of cognitive functions during childhood. *J. Cogn. Neurosci.* **16**, 1227-1233. doi:10.1162/0898929041920441

Naruse, M., Ishino, Y., Kumar, A., Ono, K., Takebayashi, H., Yamaguchi, M., Ishizaki, Y., Ikenaka, K. and Hitoshi, S. (2016). The dorsoventral boundary of the germinal zone is a specialized niche for the generation of cortical oligodendrocytes during a restricted temporal window. *Cereb. Cortex* **26**, 2800-2810. doi:10.1093/cercor/bhv141

Naruse, M., Ishizaki, Y., Ikenaka, K., Tanaka, A. and Hitoshi, S. (2017). Origin of oligodendrocytes in mammalian forebrains: a revised perspective. *J. Physiol. Sci.* **67**, 63-70. doi:10.1007/s12576-016-0479-7

Nimmerjahn, A., Kirchhoff, F. and Helmchen, F. (2005). Resting microglial cells are highly dynamic surveillants of brain parenchyma in vivo. *Science* **308**, 1314-1318. doi:10.1126/science.1110647

Okada, A., Charron, F., Morin, S., Shin, D. S., Wong, K., Fabre, P. J., Tessier-Lavigne, M. and McConnell, S. K. (2006). Boc is a receptor for sonic hedgehog in the guidance of commissural axons. *Nature* **444**, 369-373. doi:10.1038/nature05246

O'Meara, R. W., Ryan, S. D., Colognato, H. and Kothary, R. (2011). Derivation of enriched oligodendrocyte cultures and oligodendrocyte/neuron myelinating co-cultures from post-natal murine tissues. *J. Vis. Exp.* **54**, e3324. doi:10.3791/3324

Orihuela, R., McPherson, C. A. and Harry, G. J. (2016). Microglial M1/M2 polarization and metabolic states. *Br. J. Pharmacol.* **173**, 649-665. doi:10.1111/bph.13139

Ortega, F., Gascón, S., Masserdotti, G., Deshpande, A., Simon, C., Fischer, J., Dimou, L., Chichung Lie, D., Schroeder, T. and Berninger, B. (2013).

Oligodendrogliogenic and neurogenic adult subependymal zone neural stem cells constitute distinct lineages and exhibit differential responsiveness to Wnt signalling. *Nat. Cell Biol.* **15**, 602-613. doi:10.1038/ncb2736

Poggi, G., Boretius, S., Möbius, W., Moschny, N., Baudewig, J., Ruhwedel, T., Hassouna, I., Wieser, G. L., Werner, H. B., Goebbels, S. et al. (2016). Cortical network dysfunction caused by a subtle defect of myelination. *Glia* **64**, 2025-2040. doi:10.1002/glia.23039

Ransohoff, R. M. (2016). A polarizing question: do M1 and M2 microglia exist? *Nat. Neurosci.* **19**, 987-991. doi:10.1038/nn.4338

Roessler, E. and Muenke, M. (2010). The molecular genetics of holoprosencephaly. *Am. J. Med. Genet. C Semin. Med. Genet.* **154C**, 52-61. doi:10.1002/ajmg.c.30236

Samanta, J., Grund, E. M., Silva, H. M., Lafaille, J. J., Fishell, G. and Salzer, J. L. (2015). Inhibition of Gli1 mobilizes endogenous neural stem cells for remyelination. *Nature* **526**, 448-452. doi:10.1038/nature14957

Sanchez, M. A. and Armstrong, R. C. (2018). Postnatal Sonic hedgehog (Shh) responsive cells give rise to oligodendrocyte lineage cells during myelination and in adulthood contribute to remyelination. *Exp. Neurol.* **299**, 122-136. doi:10.1016/j.expneurol.2017.10.010

Sanchez-Arrones, L., Cardozo, M., Nieto-Lopez, F. and Bovolenta, P. (2012). Cdon and Boc: Two transmembrane proteins implicated in cell-cell communication. *Int. J. Biochem. Cell Biol.* **44**, 698-702. doi:10.1016/j.biocel.2012.01.019

Sanchez, M. A., Sullivan, G. M. and Armstrong, R. C. (2018). Genetic detection of Sonic hedgehog (Shh) expression and cellular response in the progression of acute through chronic demyelination and remyelination. *Neurobiol. Dis.* **115**, 145-156. doi:10.1016/j.nbd.2018.04.003

Seri, B., Herrera, D. G., Gritti, A., Ferron, S., Collado, L., Vescovi, A., Garcia-Verdugo, J. M. and Alvarez-Buylla, A. (2006). Composition and organization of the SCZ: a large germinal layer containing neural stem cells in the adult mammalian brain. *Cereb. Cortex* **16** Suppl. 1, i103-i111. doi:10.1093/cercor/bhk027

Skripuletz, T., Lindner, M., Kotsiari, A., Garde, N., Fokuhl, J., Linsmeier, F., Trebst, C. and Stangel, M. (2008). Cortical demyelination is prominent in the murine cuprizone model and is strain-dependent. *Am. J. Pathol.* **172**, 1053-1061. doi:10.2353/ajpath.2008.070850

Tenzen, T., Allen, B. L., Cole, F., Kang, J.-S., Krauss, R. S. and McMahon, A. P. (2006). The cell surface membrane proteins Cdo and Boc are components and targets of the Hedgehog signaling pathway and feedback network in mice. *Dev. Cell* **10**, 647-656. doi:10.1016/j.devcel.2006.04.004

Tomassy, G. S., Dershowitz, L. B. and Arlotta, P. (2016). Diversity matters: a revised guide to myelination. *Trends Cell Biol.* **26**, 135-147. doi:10.1016/j.tcb.2015.09.002

Tong, C. K., Fuentealba, L. C., Shah, J. K., Lindquist, R. A., Ihrie, R. A., Guinto, C. D., Rodas-Rodriguez, J. L. and Alvarez-Buylla, A. (2015). A dorsal SHH-dependent domain in the V-SVZ produces large numbers of oligodendroglial lineage cells in the postnatal brain. *Stem Cell Rep.* **5**, 461-470. doi:10.1016/j.stemcr.2015.08.013

Uhlemann, R., Gertz, K., Boehmerle, W., Schwarz, T., Nolte, C., Freyer, D., Kettenmann, H., Endres, M. and Kronenberg, G. (2016). Actin dynamics shape microglia effector functions. *Brain Struct. Funct.* **221**, 2717-2734. doi:10.1007/s00429-015-1067-y

Vuong, T. A., Leem, Y.-E., Kim, B.-G., Cho, H., Lee, S.-J., Bae, G.-U. and Kang, J.-S. (2017). A Sonic hedgehog coreceptor, BOC regulates neuronal differentiation and neurite outgrowth via interaction with ABL and JNK activation. *Cell. Signal.* **30**, 30-40. doi:10.1016/j.cellsig.2016.11.013

Wang, L. C. and Almazan, G. (2016). Cdon, a cell surface protein, mediates oligodendrocyte differentiation and myelination. *Glia* **64**, 1021-1033. doi:10.1002/glia.22980

White, R. and Krämer-Albers, E. M. (2014). Axon-glia interaction and membrane traffic in myelin formation. *Front. Cell. Neurosci.* **7**, 1-8. doi:10.3389/fncel.2013.00284

White, R., Gonsior, C., Krämer-Albers, E. M., Stöhr, N., Hüttelmaier, S. and Trotter, J. (2008). Activation of oligodendroglial Fyn kinase enhances translation of mRNAs transported in hnRNP A2-dependent RNA granules. *J. Cell Biol.* **181**, 579-586. doi:10.1083/jcb.200706164

Wolf, Y., Yona, S., Kim, K.-W. and Jung, S. (2013). Microglia, seen from the CX3CR1 angle. *Front. Cell Neurosci.* **7**, 26. doi:10.3389/fncel.2013.00026

Yam, P. T. and Charron, F. (2013). Signaling mechanisms of non-conventional axon guidance cues: the Shh, BMP and Wnt morphogens. *Curr. Opin. Neurobiol.* **23**, 965-973. doi:10.1016/j.conb.2013.09.002

Yona, S., Kim, K.-W., Wolf, Y., Mildner, A., Varol, D., Breker, M., Strauss-Ayali, D., Viukov, S., Guilliams, M., Misharin, A. et al. (2013). Fate mapping reveals origins and dynamics of monocytes and tissue macrophages under homeostasis. *Immunity* **38**, 79-91. doi:10.1016/j.immuni.2012.12.001

Young, K. M., Psachoulia, K., Tripathi, R. B., Dunn, S.-J., Cossell, L., Attwell, D., Tohyama, K. and Richardson, W. D. (2013). Oligodendrocyte dynamics in the healthy adult CNS: evidence for myelin remodeling. *Neuron* **77**, 873-885. doi:10.1016/j.neuron.2013.01.006

Yuan, A. and Nixon, R. A. (2016). Specialized roles of neurofilament proteins in synapses: Relevance to neuropsychiatric disorders. *Brain Res. Bull.* **126**, 334-346. doi:10.1016/j.brainresbull.2016.09.002

Zhang, J., Zhang, Z. G., Li, Y., Ding, X., Shang, X., Lu, M., Elias, S. B. and Chopp, M. (2015). Fingolimod treatment promotes proliferation and differentiation of oligodendrocyte progenitor cells in mice with experimental autoimmune encephalomyelitis. *Neurobiol. Dis.* **76**, 57-66. doi:10.1016/j.nbd.2015.01.006

Zuchero, J. B., Fu, M.-M., Sloan, S. A., Ibrahim, A., Olson, A., Zaremba, A., Dugas, J. C., Wienbar, S., Caprariello, A. V., Kantor, C. et al. (2015). CNS myelin wrapping is driven by actin disassembly. *Dev. Cell* **34**, 152-167. doi:10.1016/j.devcel.2015.06.011

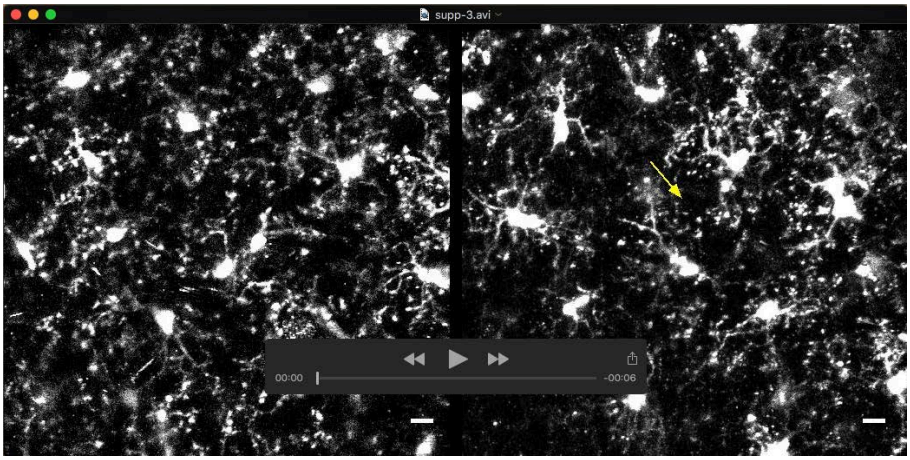

Movie 1. Movie derived from live imaging of YFP$^+$ microglia/macrophage in the cerebral cortex grey matter of CX3CR1/YFP WT and Boc mutant mice at D8. The arrow indicates a microglia/macrophage displaying one SFE in the mutant, while no SFE is detected in the WT. Scale bar: 10 µm.